

Copyright
by
Man-Fung Cheung
2011

The Dissertation committee for Man-Fung Cheung

Certifies that this is the approved version of the following dissertation:

**Gluon Propagator in Classical Color Field of Colliding
Hadrons and its Implications for Hadronic Cross
Sections**

Committee:

Charles B. Chiu, Supervisor

Duane Dicus

Oscar Gonzalez

Christina Markert

E. C. George Sudarshan

**Gluon Propagator in Classical Color Field of Colliding
Hadrons and its Implications for Hadronic Cross
Sections**

by

Man-Fung Cheung, B.Sc.

DISSERTATION

Presented to the Faculty of the Graduate School of
The University of Texas at Austin
in Partial Fulfillment
of the Requirements
for the Degree of

DOCTOR OF PHILOSOPHY

THE UNIVERSITY OF TEXAS AT AUSTIN

August 2011

Dedicated to my parents, Yan-Man Cheung and Wai-Hong Cheng,
whom every single accomplishment of mine are based upon; and
my girlfriend, Wan-Ting Chuang, who has been supportive and has shared
uncertainties, sacrifices and happiness during my graduate study.

Acknowledgments

I would like to take this opportunity to thank all the kind people I have encountered during my graduate study.

First and foremost, I would like to express my cordial gratitude to my advisor, Prof. Charles Chiu, for his timeless support on my study. His guidance and criticisms are crucial to sharpen my thoughts and my understanding of physics. From him, I learnt how to examine thoughts and convey ideas. The patience and motivation he has provided to me are both qualitatively and quantitatively immeasurable. I hope one day I would be as good a teacher and an advisor as Dr. Chiu is. I feel truly fortunate to have him as my advisor.

I would like thank my dissertation committee members, Prof. Duane Dicus, Prof. Oscar Gonzalez, Prof. Christina Markert and Prof. E. C. George Sudarshan, for their insightful comments and questions that help improve my dissertation, especially for the valuable discussions I had with Dr. Dicus and Dr. Sudarshan throughout my study.

Prof. Austin Gleeson's teaching philosophy has been very influential to me when I was an assistant instructor. I thank him for his advices and giving me freedom to design my course. My thanks also go to the group of assistant instructors working with me. It has been a pleasure to share our teaching experience to each other.

I thank Matt Haley, also a student of Dr. Chiu, for his moral and mutual support, especially when both of us had a difficult time, and also for his help on improving my writing. In addition, to my friends who helped me along the way and shared many good times with me, I truly value our friendship.

Last but not least, this chapter of my life will not be completed without the constant love, concern and support from my family and my girlfriend whom this dissertation is dedicated to. I cannot thank them enough.

Gluon Propagator in Classical Color Field of Colliding Hadrons and its Implications for Hadronic Cross Sections

Publication No. _____

Man-Fung Cheung, Ph.D.
The University of Texas at Austin, 2011

Supervisor: Charles B. Chiu

We review the Regge theory and the minijet model for pp and $\bar{p}p$ collisions. We show that, in the conventional minijet approach, the asymptotic behavior of the total cross section calculated using currently accepted gluon distribution function and perturbative QCD rises too rapidly when compared with the data and fails to satisfy Froissart bound. To tame the rise, we have developed a new formalism for the interaction between QCD gluon and the classical color field of the colliding nucleons, and show how the gluon propagator is modified. The corresponding gauge invariance condition of the propagator is derived and shown to be satisfied. The modified gluon propagator leads to a suppression of the minijet cross section due to the $gg \rightarrow gg$ subprocess in the small- x region. We show that the pp and $\bar{p}p$ total cross section from $\sqrt{s} = 5$ GeV to 30 TeV can be described as a sum of a hard component contributed by the classical field modified minijet model and a soft component

due to the exchange of the Pomeron and the $I = 0$ exchange-degenerate ω and f Regge trajectories. The soft-component model is motivated by the notion of duality. The predicted total cross section has a $\ln s$ asymptotic behavior.

Table of Contents

Acknowledgments	v
Abstract	vii
List of Tables	xii
List of Figures	xiii
Chapter 1 Introduction	1
1.1 Strong Interaction	1
1.2 Quantum Chromodynamics (QCD)	2
1.3 Proton-Proton and Anti-Proton-Proton Total Cross Section	3
Chapter 2 Regge Theory and Duality	8
2.1 Crossing Symmetry	8
2.2 Regge Pole Trajectory in pp	10
2.3 Exchange Degeneracy in pp and $\bar{p}p$	14
2.4 Nonexotic and exotic quantum numbers	17
2.5 Finite Energy Sum Rule (FESR)	18
2.6 Duality Diagram	20
Chapter 3 Minijet	24
3.1 QCD-inspired minijet	25
3.2 Violation of Froissart bound	29
3.3 Taming the rise	29
3.4 Minijet in classical color field	31

Chapter 4	Classical Effective Theory of Small-x Gluons	35	
4.1	Why does $g(x, Q^2)$ rise?	35	
4.2	Space-time structure of partons	37	
4.3	Classical field of a nucleon	37	
4.4	The McLerran-Venugopalan model	41	
Chapter 5	Quantum Gluon Propagator in Classical Field	44	
5.1	Lagrangian in classical field	44	
5.2	Quantum theory	46	
5.3	Propagator	48	
5.3.1	$\langle A^{a+} A^{b+} \rangle_{MV}$	50	
5.3.2	1-1 term	51	
5.3.3	1-2 and 2-1 terms	54	
5.3.4	2-2 term	54	
5.3.5	Result	55	
Chapter 6	Implications for Hadronic Cross Sections	57	
6.1	Application to minijet	57	
6.2	Analytic continuation	59	
6.3	Resummation	62	
6.4	Modification factor in Minijet	63	
Chapter 7	Result and Discussion	65	
7.1	pp and $\bar{p}p$ total cross section at high energy from modified minijet model	65	
7.2	Asymptotic behavior of the σ_{mnj}^{cl} and the $J = 1 + \lambda$ relationship	67	
7.3	Why is minijet production suppressed in the small x region?	69	
7.4	Minijet cross section of pA and AA	70	
Chapter 8	Summary	71	
	Appendices	76	
	Appendix A	Light-cone Coordinate	77

Appendix B	Gauge Invariance	79
B.1	Gauge transformation with background	79
B.2	Slavnov-Taylor Identity	81
B.3	Gauge invariance of the modified propagator	87
B.3.1	Terms linear in \mathcal{L}_{int_1} and \mathcal{L}_{int_2}	89
B.3.2	Checking gauge invariant	90
Bibliography		94

List of Tables

1.1	Table of typical pp and $\bar{p}p$ total cross sections from different colliders	5
-----	--	---

List of Figures

1.1	Energy dependence of $\bar{p}p$ and pp total cross section. The data is from [1].	4
1.2	Comparing the rise of total cross section and that of minijet cross section. The data points are the total cross section. The shaded area is represents the contribution from the jet calculation. Notice that the rise of the total cross section and the rise of the shaded area behaves similarly. Figure is obtained from Ref. [2].	6
2.1	(a) The s-channel scattering process: $1 + 2 \rightarrow 3 + 4$ and (b) the t-channel scattering process: $1 + \bar{3} \rightarrow \bar{2} + 4$	10
2.2	Integration contours of the Sommerfeld-Watson transformation in the complex l -plane.	12
2.3	The Chew-Frautschi plot of ω and f trajectories. Ref: [3] . . .	15
2.4	A illustration of FESR from [4].	19
2.5	A illustration of (a) meson-meson and (b) meson-baryon s-t channel duality.	21
2.6	A illustration of $\bar{p}p$ s-t channel duality.	23
3.1	ZEUS result [5] of various pdf at $Q^2 = 10 \text{ GeV}^2$. Note that the gluon and sea quark pdfs in the plot are only 5% of their actual values.	27
3.2	Comparison between the mini-jet cross section calculated with the full gg elastic differential cross section (solid line) and that calculated with the last two terms in (3.6) (dashed line). . . .	28
3.3	A picture of a nucleon in the $\frac{1}{x} - Q^2$ plane.	32
5.1	Feynman diagram of the propagator in classical field. Each vertex can be \mathcal{L}_{int_1} or \mathcal{L}_{int_2} . The dotted line represents the interaction the momentum exchange between the gluon and the classical field.	50

6.1	Momentum conservation of the vertex and on-shell condition for the incoming(x_1P^+) and outgoing(k) gluons: $-2x_1P \cdot q + q^2 = 0 \Rightarrow q^- = q^2/(2x_1P^+)$	58
6.2	Schematic Feynman diagram which represents the iterative sum of the modified propagator. The first term is the bare propagator. The blob and the two lines connecting to it in the series represent the interaction between the quantum gluon propagator and the classical field.	63
6.3	x_1 -dependence of F_{mnj}^{cl} while keeping $x_2 = 1$	64
7.1	Comparison between pp and $\bar{p}p$ data with classical field modified minijet model. Curves a and b are σ_{pp} and $\sigma_{\bar{p}p}$ of the present model where Q_s^2 is defined in eq. (7.4) and (7.5), with $\lambda = 0.28$. Curves c and d are for σ_{pp} with $\lambda = 0.25$ and 0.33 , respectively. Curve e is the original minijet model with $F_{mnj} = 1$. The data is from [1].	67
B.1	Schematic Feynman diagram for gluon GF with single interaction with A	89

Chapter 1

Introduction

1.1 Strong Interaction

Among the four fundamental interactions of nature: the electromagnetic force, the weak force, the strong force and the gravitational force, the strong force, also called the strong interaction, as the name suggested is the strongest. It is so strong that it overcomes the electromagnetic repulsion due to the same charged protons to form a nucleus. Further down to the microscopic level, the strong interaction is also responsible for the existence of hadrons, including mesons and baryons. It is responsible for the binding of quark and anti-quark into mesons, and the binding of three quarks into baryons. Stable hadrons are commonly used in collider experiments in many world leading laboratories, including CERN, Fermilab and Brookhaven National Lab, to explore the energy frontier of nature. A better theoretical understanding of the strong interaction leads to more precise interpretations of the experimental results. In turn, much improved theory can be derived from the experiments.

1.2 Quantum Chromodynamics (QCD)

It is generally accepted that the strong interaction is described by quantum chromodynamics (QCD) in which quarks and gluons are fundamental particles carrying color charge and the interaction is mediated by gluons. This belief is mainly based on the successful description of the processes involving large momentum transfer. These processes are called hard processes.

One profound consequence of QCD is the asymptotic freedom [6, 7] which means the coupling between two strongly interacting particles tends to be zero as their momentum transfer approaches infinity. Asymptotic freedom validates the use of perturbation theory in hard process. However, hadronic collisions cannot be described by pQCD alone. Soft processes, in which small momentum transfer is involved, are prevalent in hadronic collisions.

Soft process is difficult to handle in general because

- its coupling is strong so that perturbative method is not valid;
- its dynamics is governed by non-linear equation.

One way to treat the effect due to the soft processes is through the application of factorization in parton model (for review, see [8]) in which the hadron-hadron cross section is written schematically as

$$\sigma = \sum_{i,j} \int dx_1 dx_2 dQ^2 f_{p_i/A}(x_1, \mu^2) f_{p_j/B}(x_2, \mu^2) H(x_1, x_2, Q^2, \mu^2), \quad (1.1)$$

where $f_{p_i/A}(x_1, \mu^2)$, $(f_{p_j/B}(x_2, \mu^2))$, is the parton distribution function of parton- i with momentum fraction x_1 from hadron A, (parton- j from hadron B), evaluated at scale μ^2 and H is the hard scattering cross section of the parton-parton sub-process with momentum exchange at Q^2 . The renormalization scale μ^2 serves as a division line between soft and hard. The hard part only consists of processes with momentum larger than $Q^2 > \mu^2$, while all the soft scattering with $Q^2 < \mu^2$ is absorbed into $f_{p_i/A}$. One can measure $f_{p_i/A}$ at a fixed μ^2 higher than the QCD scale Λ_{QCD} , then $f_{p_i/A}$ at a higher μ^2 can be calculated using pQCD. In this parton model, the scattering process becomes incoherent, namely one parton does not interfere with the hard scattering of other partons. However, the conventional description of the gluon distribution in high energy grows rapidly. One expects the non-linearity of QCD implies the recombination of gluons. Thus, the gluon distribution will saturate at high energy. According to the analysis of the HERA data [9], there emerges a saturation scale Q_s^2 below which the gluon inside the hadron is saturated. So far, how to describe a saturated hadron is still an open question.

1.3 Proton-Proton and Anti-Proton-Proton Total Cross Section

One of the unsettled and interesting issues in the strong interaction is the understanding of total cross section of antiproton-proton $\bar{p}p$ and proton-proton pp collisions at high energy. These total cross sections were measured over a large range of center-of-mass energy, \sqrt{s} . See Fig. 1.1

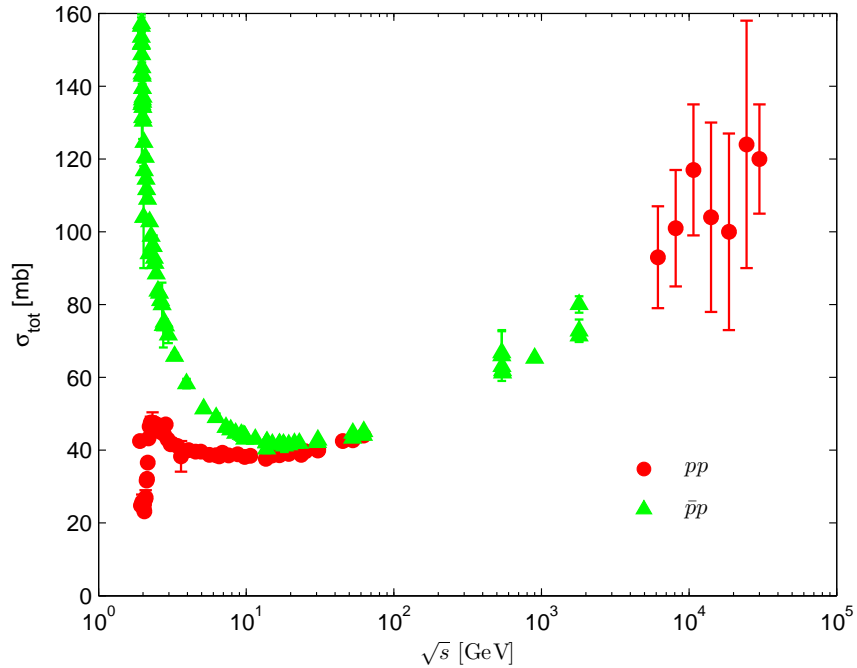


Figure 1.1: Energy dependence of $\bar{p}p$ and pp total cross section. The data is from [1].

By mid 60s, the pp cross section was already well measured from $\sqrt{s} = 2$ to 6.3 GeV. In this energy region, the pp cross section is almost constant throughout at the value ~ 38 mb. At the time one thought that the pp cross section has already reached some constant asymptotic value [10]. In the same energy region the $\bar{p}p$ cross section drops from 90 mb to 60 mb. The trend suggests that as the energy further increases, eventually $\bar{p}p$ cross section could approach a common asymptotic value as the pp cross section as implied by the Pomeranchuk theorem [11].

Along with the availability of higher energy accelerators, as time went

on, higher energy data became available [1]. Experiments have confirmed that $\bar{p}p$ cross section merges with the pp cross section at around $\sqrt{s} = 50$ GeV. Beyond which, they both can be described by the same energy dependent function which continues to rise as the energy further increases. Some typical examples are listed in Table 1.1. Various theoretical interpretations and models

Experiment	\sqrt{s}	σ_{tot}
ISR(pp)	62.7 GeV	43.82 ± 0.23 mb
SPS($p\bar{p}$)	541 GeV	63.0 ± 2.1 mb
Tevatron(CDF, $p\bar{p}$)	1.8 TeV	80.03 ± 2.24 mb
Cosmic ray (pp)	30 TeV	120 ± 15 mb

Table 1.1: Table of typical pp and $\bar{p}p$ total cross sections from different colliders have been developed in attempt to understand the rise of the pp and $\bar{p}p$ cross sections from ISR energies and beyond.

In the 60s and 70s, there was an extensive development of Regge theory which provides a useful framework for the description of soft physics, especially near zero-momentum-transfer. It is not a fundamental theory as QCD. However in practice in the kinematic domain beyond the reach of pQCD, Regge theory provides a supplementary tool in the description of soft physics. In our work, we will divide the total cross section into a soft component and a hard component. Regge theory will be used in the description of the soft component.

Another approach is the QCD-inspired minijet model. It is first noticed by Cline et al. [2] that the energy dependence of the total cross section rises very similarly to the cross section of jet with small invariance mass, called

minijet, calculated by QCD. See Fig. 1.2. However, as energy keeps on increasing, the minijet cross section rises too rapidly. Various approaches based on eikonal models were then developed to tame the rise. Typically in these approaches, the fittings of the data are successful only up to a certain energy, as the energy further increases the predicted curve would begin to predict too rapid a rise.

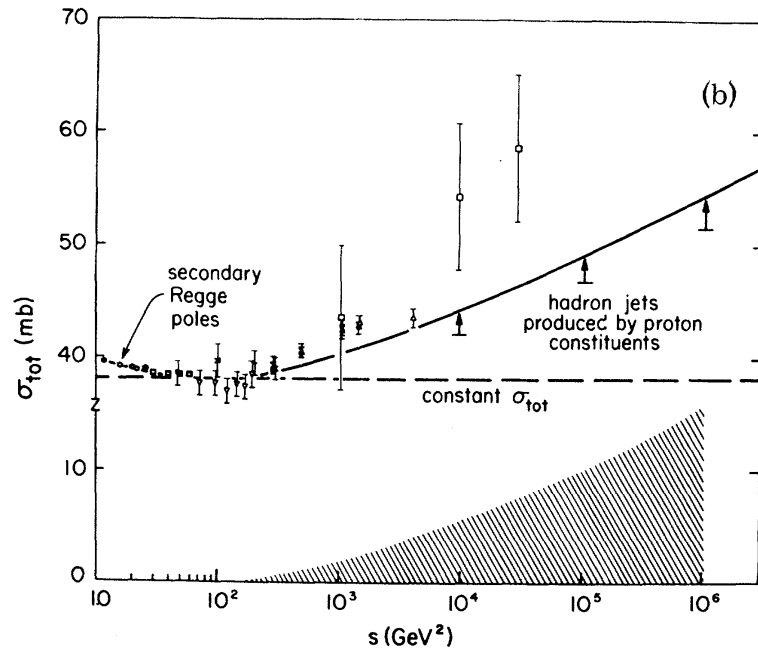


Figure 1.2: Comparing the rise of total cross section and that of minijet cross section. The data points are the total cross section. The shaded area represents the contribution from the jet calculation. Notice that the rise of the total cross section and the rise of the shaded area behaves similarly. Figure is obtained from Ref. [2].

Recently, a new approach, called Color Glass Condensate (CGC), was developed to treat the non-perturbative part of QCD by formulating the dy-

namics of saturated gluon field in terms of a classical field theory derived from the QCD Lagrangian. The idea of CGC is initiated by McLerran and Venugopalan. Their model is referred to as the MV model.

In this work, we applied the MV model to the pQCD calculation of the $\bar{p}p$ and pp total cross sections within the framework of QCD. We derived the modified gluon propagator in the presence of the classical color field and found that it provides the right amount of taming on the minijet cross section. Here the minijet cross section only rise as $\ln s$ asymptotically. This $\ln s$ dependence satisfies the Froissart bound [12, 13] which requires that any total cross section has to satisfy $\sigma \leq \text{constant} \times (\ln s)^2$.

This dissertation is organized as the followings. A short review of Regge theory and its implications for the $\bar{p}p$ and pp cross section will be presented in Chapter 2. We discuss the conventional minijet model and its problem in Chapter 3. An introduction of classical color field in nucleon collision will be given in Chapter 4. Chapter 5 is devoted to the calculation of the classical field modified gluon propagator then it is applied to minijet cross section in Chapter 6. The implication of the modified propagator for the minijet cross section is presented in Chapter 7. The gauge invariance of propagator is discussed in Appendix B. We conclude the present model and give a outlook of the possible applications of the present model on other hadronic processes in Chapter 8.

Chapter 2

Regge Theory and Duality

As we mentioned in Chapter 1, the pp and $\bar{p}p$ total cross sections, σ_{pp} and $\sigma_{\bar{p}p}$, at low energy, $\sqrt{s} \lesssim 30$ GeV, can be effectively described by Regge theory. In this chapter, we will review the main ingredients of Regge theory that lead to (a) the absence of energy dependence in σ_{pp} and (b) the $1/\sqrt{s}$ power law dependence of $\sigma_{\bar{p}p}$ in that region. We will also review the duality principle in strong interaction which plays an important role in the application of Regge theory.

2.1 Crossing Symmetry

We first consider the process $1 + 2 \rightarrow 3 + 4$, where the particles have masses m_i and momentum p_i for $i = 1, 2, 3$ and 4 . We use the metric $(+, -, -, -)$ such that

$$p_1^\mu p_{2\mu} = E_1 E_2 - \vec{p}_1 \cdot \vec{p}_2. \quad (2.1)$$

The Lorentz invariant Mandelstam variables s , t and u are defined by

$$\begin{aligned} s &= (p_1 + p_2)^2 \\ t &= (p_1 - p_3)^2 \\ u &= (p_1 - p_4)^2 \end{aligned} \tag{2.2}$$

that they satisfy

$$s + t + u = \sum_{i=1}^4 m_i^2. \tag{2.3}$$

The s-channel scattering amplitude, shown in Fig. 2.1(a), is a function of only two independent variables, denoted by $A_{12,34}(s, t) \equiv \langle 34|T|12 \rangle$. If we flip the sign of the momentum of 2 and 3 and replace particle 2 and 3 by their antiparticle, $\bar{2}$ and $\bar{3}$, the process become $1 + \bar{3} \rightarrow \bar{2} + 4$. Its scattering amplitude is $A_{1+\bar{3},\bar{2}+4}(s', t')$. The original variable $t = (p_1 - p_3)^2$ in Fig. 2.1(a) acts as the total squared energy $s' = (p'_1 + p'_3)^2 = (p_1 - p_3)^2 = t$ in Fig. 2.1(b). The process $1 + \bar{3} \rightarrow \bar{2} + 4$ is called the t-channel process of $1 + 2 \rightarrow 3 + 4$. Even though the variables of the two channel are related, the amplitudes are defined in different region of the variables. For the s-channel, the physical region is given by $s \geq (m_1 + m_2)^2$ and $t \leq 0$, while the physics region for the t-channel is $s' = t \geq (m_1 + m_3)^2$ and $t' = s \leq 0$. Those are disconnected regions.

In the framework of S-matrix theory, the basic assumption is that the amplitudes of these two different channels are represented by one single analytic function. The relation between the amplitudes of two channels is given by

$$A_{12,34}(s, t) = A_{1\bar{3},\bar{2}4}(s' = t, t' = s). \tag{2.4}$$

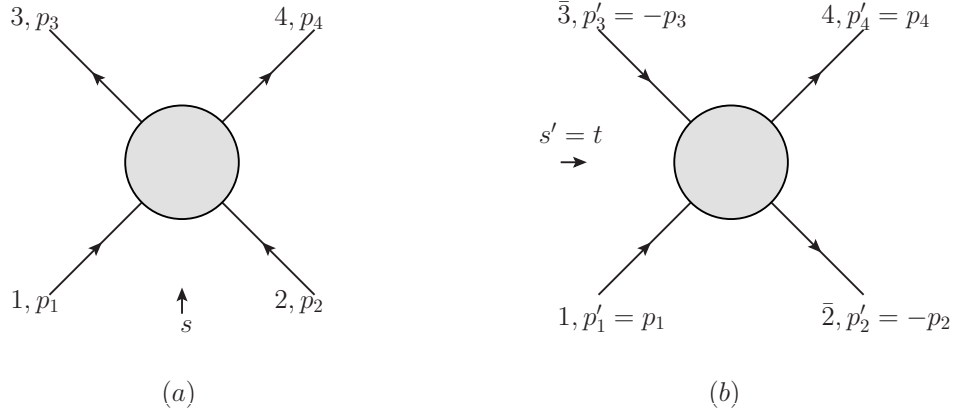


Figure 2.1: (a) The s-channel scattering process: $1 + 2 \rightarrow 3 + 4$ and (b) the t-channel scattering process: $1 + \bar{3} \rightarrow \bar{2} + 4$.

This assumption enable us to write the amplitude in any convenient channel and then analytical continue to other region to represent processes in other channels.

2.2 Regge Pole Trajectory in pp

Let's first consider the pp elastic process: $p_1 p_2 \rightarrow p_3 p_4$ with $m_i = m$. In the t-channel, it becomes $p_1 \bar{p}_3 \rightarrow \bar{p}_2 p_4$. We write the amplitude in partial wave expansion as

$$A_{pp}(s, t) = 16\pi \sum_{l=0}^{\infty} (2l + 1) A_l(t) P_l(z_t), \quad (2.5)$$

where P_l is the Legendre polynomial of the first kind and $z_t = 1 + 2s/(t - 4m^2)$. We can further rewrite (2.5) into a sum of even- and odd-signatured

amplitudes, respectively denoted by A^+ and A^- , such that

$$A_{pp}(s, t) = A^+(s, t) + A^-(s, t), \quad (2.6)$$

where

$$A^\pm(s, t) = 8\pi \sum_{l=0}^{\infty} (2l+1) A_l^\pm(t) (P_l(z_t) \pm P_l(-z_t)). \quad (2.7)$$

Since $P_l(-z) = (-1)^l P_l(z)$, A^+ and A^- are the sums of term with only even l and only odd l , respectively. One can generalize l of $A_l^\pm(t)$ from a non-negative integer to a complex number such that the partial wave amplitude in complex l matches the original value when l is non-negative integers,

$$A^+(l, t) = A_l^+(t) \quad \text{for even } l \quad (2.8)$$

$$A^-(l, t) = A_l^-(t) \quad \text{for odd } l \quad (2.9)$$

The sum in eq. (2.7) can be written as a contour integral of l , called the Sommerfeld-Watson transformation [14], as

$$A^\pm(s, t) = 4\pi i \oint_C dl (2l+1) A^\pm(l, t) \frac{P_l(-z_t) \pm P_l(z_t)}{\sin(\pi l)}, \quad (2.10)$$

where the contour C surrounds all the pole from $1/\sin(\pi l)$ the real axis from 0 to ∞ in a clockwise direction as shown in Fig. 2.2(a), such that, for any function $f(z)$ analytic along the positive real axis, we have

$$\oint_C dz \frac{f(z)}{\sin(\pi z)} = \frac{i}{2} \sum_{l=0}^{\infty} (-1)^l f(l). \quad (2.11)$$

According to Forissart-Gribov Formula, the behavior of the amplitude $A^\pm(l, t)$ at large l goes like

$$A^\pm(l, t) \sim l^{-\frac{1}{2}} z_t^{-l}. \quad (2.12)$$

In the asymptotic energy region, large s , the integrand of eq. (2.10) goes to zero at large l . It allows us to deform the contour to C' that l goes from $-1/2 - i\infty$ to $-1/2 + i\infty$. If $A^\pm(l, t)$ has poles in the right l -plane, we pick up the residue contribution from the pole as shown in Fig. 2.2(b).

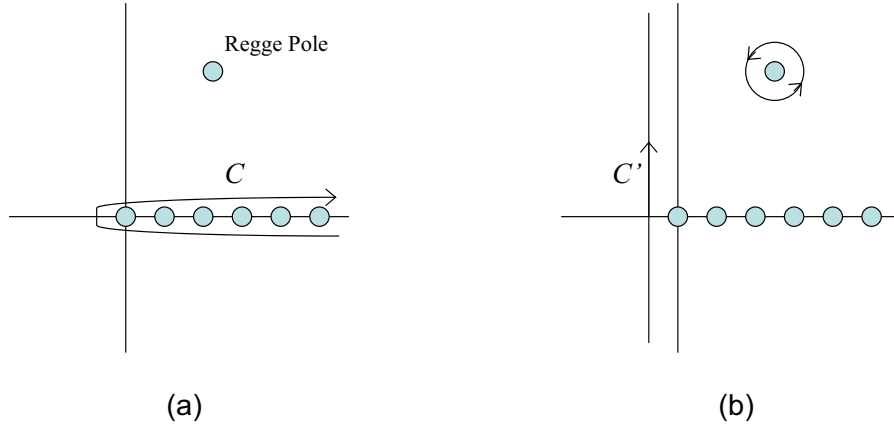


Figure 2.2: Integration contours of the Sommerfeld-Watson transformation in the complex l -plane.

In the Regge theory, it is assumed that in the t -channel the resonances contribute collectively as a family with either even or odd l . The members of the family lie on a trajectory on the complex l -plane. The trajectory is called the Regge trajectory $\alpha^\pm(t)$ and has the property that when t equals the mass of a resonance member, $t = m_R^2$, the value of $\alpha^\pm(t)$ equals to the angular

momentum of the resonance, i.e.

$$\alpha^\pm(t = m_R^2) = l_R, \quad (2.13)$$

where $+$ and $-$ label the signature of Regge trajectory with even and odd l , respectively. An other assumption is that a simple pole, called Regge pole, is assigned to the partial wave amplitude $A^\pm(l, t)$ at the position of a Regge trajectory on the l -plane. The residue of the Regge pole is $\beta^\pm(t)$.

With the consideration of the Regge pole, eq. (2.10) becomes

$$\begin{aligned} A^\pm(s, t) = & -8\pi \sum_i \frac{(2\alpha_i^\pm(t) + 1)\beta_i^\pm(t)}{\sin(\pi\alpha_i^\pm(t))} (P_{\alpha_i^\pm(t)}(-z_t) \pm P_{\alpha_i^\pm(t)}(z_t)) \\ & + 4\pi i \int_{-1/2-i\infty}^{-1/2+i\infty} dl (2l + 1) A^\pm(l, t) \frac{P_l(-z_t) \pm P_l(z_t)}{\sin(\pi l)} \end{aligned} \quad (2.14)$$

The first term is the sum of all Regge pole i . The second term is referred as the "background integral" which can be diminished such that it is negligible compared to the Regge pole term at large s [15]. The amplitude is first written in t -channel, where $t > 4m^2$ and $s \leq 0$. However, eq. (2.14) allows us to continue the expression to the high energy s -channel, $s > 4m^2$ and $t \leq 0$. Large positive s corresponds to large negative z_t . The asymptotic behavior of the Regge term of eq. (2.14) is

$$A^\pm(s, t) \sim \sum_i \beta_i^\pm(t) \Gamma(-\alpha_i^\pm(t)) (1 \pm e^{-i\pi\alpha_i^\pm(t)}) \left(\frac{s}{s_0}\right)^{\alpha_i^\pm(t)}, \quad (2.15)$$

where the factor $1 \pm e^{-i\pi\alpha_i^\pm(t)}$ is the signature factor coming from rewriting $(-1)^\alpha = e^{-i\pi\alpha}$ in the Legendre polynomial.

The total cross section of two particle scattering can be calculated directly with the imaginary part of the elastic forward scattering amplitude using the optical theorem which says

$$\sigma_{tot} = \frac{1}{s} \text{Im}A(s, t = 0). \quad (2.16)$$

When there is the exchange of a number of Regge poles, the total cross section is the sum of the Regge pole contributions at $t = 0$ and the asymptotic behavior of the total cross section is determined a power law $s^{\alpha(0)-1}$ with the exponent given by the largest value of $\alpha(t = 0)$ among the all Regge poles exchanged.

2.3 Exchange Degeneracy in pp and $\bar{p}p$

For pp , one assumes there are three dominant Regge trajectories: the Pomeron, the ω and the f trajectories. The Pomeron is not observed as a resonance particle. It is commonly assumed to carry a vacuum quantum number and to have $\alpha_P(0) = 1$. So it contributes a constant term in σ_{tot} . The f have even signature and the ω is odd. Both ω and f trajectories are observed with $\alpha_\omega(0) \approx \alpha_f(0) \approx 1/2$ and surprisingly close to each other. Fig. 2.3 shows that both the ω trajectory $\{\omega(780), \omega_3(1670)\}$ and f trajectory $\{f_2(1270), f_4(2050)\}$ lie on a straight line. We assume their trajectories are exchange-degenerated trajectories, which are defined to have their $\alpha(t)$ and their residue $\beta(t)$ to be exactly the same. This assumption ensures that the coefficient of the two Regge contribution is almost the same except their

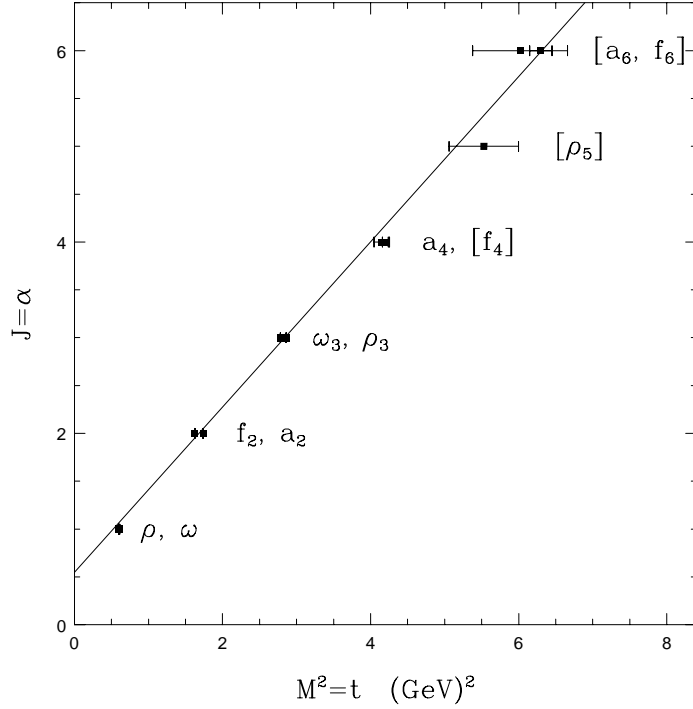


Figure 2.3: The Chew-Frautschi plot of ω and f trajectories. Ref: [3]

signature. The sum of the two Regge contribution in eq. (2.15) gives

$$\begin{aligned} \text{Im}(A_\omega(s, 0) + A_f(s, 0)) &\sim \text{Im} \left[(1 + e^{-i\pi/2}) + (1 - e^{-i\pi/2}) \right] s^{-1/2} \\ &= \text{Im}[2s^{-1/2}] = 0 \end{aligned} \quad (2.17)$$

Therefore, the total cross section of pp is only given by the Pomeron constant contribution,

$$\sigma_{tot}^{pp} = \text{Im} [A_P(s, 0) + A_\omega(s, 0) + A_f(s, 0)] / s = C_P s^{\alpha_P(0)-1} = C_P \quad (2.18)$$

A different situation emerges in the case of $\bar{p}_1 p_2 \rightarrow \bar{p}_3 p_4$. The corresponding t -channel is $\bar{p}_1 p_3 \rightarrow \bar{p}_2 p_4$. If the t -channel resonance is ω , we write

the amplitude due to ω -exchange as

$$A_{\omega}^{\bar{p}p} = \langle \bar{p}_1 p_3 | \omega \rangle \langle \omega | \bar{p}_2 p_4 \rangle. \quad (2.19)$$

We insert a pair of charge conjugation operator in between $\langle \bar{p}_1 p_3 | \omega \rangle$ and use the fact that ω has charge conjugation $C = -1$. The $\bar{p}p$ amplitude becomes

$$\begin{aligned} A_{\omega}^{\bar{p}p} &= \langle \bar{p}_1 p_3 | CC | \omega \rangle \langle \omega | \bar{p}_2 p_4 \rangle \\ &= -\langle p_1 \bar{p}_3 | \omega \rangle \langle \omega | \bar{p}_2 p_4 \rangle \\ &= -A_{\omega}^{pp}, \end{aligned} \quad (2.20)$$

since the t -channel ω -exchange for pp is $1 + \bar{3} \rightarrow \omega \rightarrow \bar{2} + 4$. Therefore, if the resonance exchange in t -channel has odd C -parity, the amplitudes of pp and $\bar{p}p$ have an opposite sign. If the resonance has even C -parity, for example f , then the amplitudes of pp and $\bar{p}p$ is the same.

The amplitude of $\bar{p}p$ due to ω and f written in term of the amplitude of pp is

$$\begin{aligned} \text{Im}(A_{\omega}^{\bar{p}p}(s, 0) + A_f^{\bar{p}p}(s, 0)) &= \text{Im}(-A_{\omega}^{pp}(s, 0) + A_f^{pp}(s, 0)) \\ &\sim \text{Im}[-(1 + e^{-i\pi/2}) + (1 - e^{-i\pi/2})] s^{-1/2} \\ &= \text{Im}[-2e^{-i\pi/2} s^{-1/2}] \\ &= 2s^{-1/2} \end{aligned} \quad (2.21)$$

Unlike total cross section of pp , here the imaginary parts of ω and f contribution do not cancel. The total cross section of $\bar{p}p$ consists of a constant term

from the Pomeron and an $1/\sqrt{s}$ term from the exchange-degenerated trajectories. It leads to the different energy behaviors between pp and $\bar{p}p$ at the low energy shown in Fig. 1.1. We will use the parameterization

$$\text{for } pp : \sigma_{soft}^{pp} = \sigma_P \quad (2.22)$$

$$\text{for } \bar{p}p : \sigma_{soft}^{\bar{p}p} = \sigma_P + \frac{c}{\sqrt{s}} \quad (2.23)$$

to fit the data with at low energy.

2.4 Nonexotic and exotic quantum numbers

The use of the exchange degenerate Regge poles leading to the parameterization of eq (2.22) and (2.23) is based on the duality principle in strong interaction physics developed in the latter part of 1960's. At the time the projectile momentum range accessible to the experiments is $p_{lab} = 5 - 30$ GeV/c, or $\sqrt{s} \sim 3-8$ GeV. In this energy range, there are two distinct sets of energy dependence in the total cross sections. There is the set of K^+p , K^+n , pp and pn scatterings where the total cross sections are approximately constant in energy, while the other set of K^-p , K^-n , $\bar{p}p$ and $\bar{p}n$ and $\pi^\pm p$ scatterings, the total cross sections fall off with energy. Why should the energy dependence of these two sets are so different? Is there any fundamental reason which distinguishes these two sets? [16]

It turned out all the cases with a constant cross section correspond to those initial scattering states which have exotic quantum numbers, i.e. they do not have the quantum number of ordinary hadrons, which are made out

of $q\bar{q}$ or qqq with nonexotic quantum numbers. This suggests that, from the direct channel point of view, the cross section can be written as a sum of two contributions, the background (or non-resonance) contribution and the resonance contribution. The former, such as the pp case, has a flat cross section which is associated with the asymptotic behavior of the exchange of Pomeron with $\alpha_P(0) = 1$. This leads to the parameterization of eq. (2.22). The nonexotic case, such as the $\bar{p}p$ case, has, in addition to the background part, also an energy dependent part which leads to the falling of the cross section of the form of eq.(2.23).

2.5 Finite Energy Sum Rule (FESR)

The relationship between the s-channel resonances and the t-channel Regge poles can be expressed in terms of FESR [16, 17]. The generic form of the n -th moment sum rule is given by

$$\int_0^N \nu^n \text{Im}A(\nu, t) d\nu = \sum_i \frac{\beta_i(t) N^{\alpha_i+1+n}}{\alpha_i + 1 + n} \quad (2.24)$$

where $\nu = \frac{s-u}{2M}$ with M being the mass of the target. The RHS is summing over the contributions of the t-channel exchange of Regge poles. For total cross section, we will only be concerned about the amplitude at $t = 0$ and omit t in the argument. We will separate the full cross section as the sum of the background associated with the Pomeron contribution, and the resonance contribution associated with the t -channel nonexotic Regge trajectory

contribution. This leads to two FESRs,

$$\int_0^N \nu^n \text{Im} A_{bk}(\nu) d\nu \sim \beta_P \frac{N^{\alpha_P+1+n}}{\alpha_P+1+n} \quad (2.25)$$

$$\int_0^N \nu^n \text{Im} A_{res}(\nu) d\nu \sim \sum_R \beta_R \frac{N^{\alpha_R+1+n}}{\alpha_R+1+n} \quad (2.26)$$

An illustration of the relationship of eq. (2.26) for the $\pi N \rightarrow \pi N$ case, where the t-channel isospin $I = 1$ is shown in Fig. 2.4 [4]. Here the t-channel ρ trajectory contribution shows the average of the oscillations of the s-channel resonance contribution.

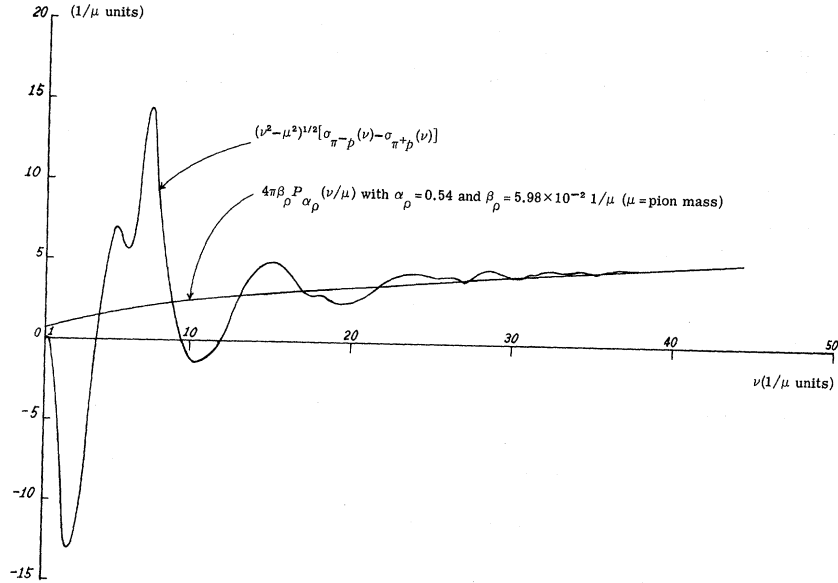


Figure 2.4: A illustration of FESR from [4].

Thus in the context of FESR, it is the absence of nonexotic resonances in the s-channel which through FESR "causes" the cancellation of the imag-

inary parts of the ω and f contributions. In this manner, FESR provides the reason for having the exchange degenerate conditions, i.e. $\beta_\omega = \beta_f$ and $\alpha_\omega(0) = \alpha_f(0)$.

2.6 Duality Diagram

The notion of duality is an important dynamical principle which is found to work at least approximately in strong interaction physics. In a perturbation theory, one can add the s-channel exchange Feynman diagram to t-channel exchange Feynman diagram to arrive at a resultant amplitude.

In contrast to this additive property in the perturbation theory, duality principle implies that when integrating over the energy dependent part of $ImA(\nu)$, it should be evaluated either in term of the s-channel resonance contribution as given on the LHS of the FESR, or in terms of t-channel Regge pole contribution i.e. the RHS of the FESR. If one takes the sum of the both channel contributions, there will be a double counting.

The duality principle has been demonstrated by the Veneziano model [18]. It involves the $\pi\pi \rightarrow \pi\omega$ scattering amplitude which is symmetric between any two pair of the Mandelstam variables, st , tu and us . The amplitude is given by the some of three terms, where each term involves a pair. For example, take the st term which can be written as a sum of s -channel pole contributions, and alternatively as a sum of the t -channel pole contributions.

One can also characterize duality relationship in terms of duality dia-

gram as shown in Fig. 2.5 [19, 20]. They are planar diagrams. Notice that for meson-meson scattering amplitude as shown in Fig. 2.5a, the s -channel nonexotic resonances build up t -channel nonexotic Regge poles. For the meson-baryon case, there is the nonexotic Regge pole, which is dual to the nonexotic baryon resonances, as it is in the case shown in Fig. 2.5b. The FESR plot of Fig. 2.4 is a special case of Fig. 2.5b, where the average behavior of the s -channel resonances is described by a smooth curve, which is the t -channel ρ trajectory.

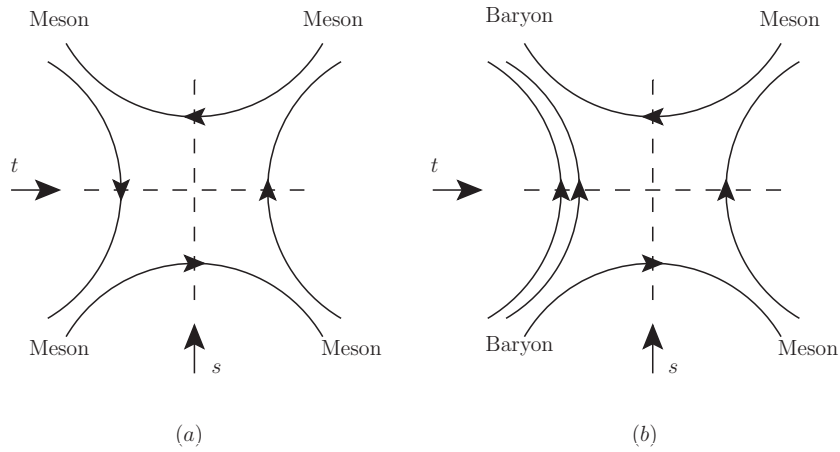


Figure 2.5: A illustration of (a) meson-meson and (b) meson-baryon s-t channel duality.

We now come to the present case of pp and $\bar{p}p$. In our work there is no explicit mentioning of how the s -channel resonances build up the asymptotic behavior, of the ω and f Regge poles. In fact the $N\bar{N}$ case has been regarded by previous authors as a puzzle in the implementation of duality principle [19, 20]. Let us look at the situation more closely.

The corresponding planar diagrams are shown in Fig. 2.6. There are two duality diagrams. In Fig. 2.6a, the s -channel resonance is nonexotic and t -channel resonance is exotic. In Fig. 2.6b, the s -channel resonance is exotic and t -channel resonance is nonexotic. For this case FESR of the zero-th moment reads

$$\int_0^N [\text{Im}A_{exotic}^{res} + \text{Im}A_{nonexotic}^{res}]d\nu \sim \left[\beta_{nonexotic} \frac{N^{\alpha_R}}{\alpha_R + 1} + \beta_{exotic} \frac{N^{\alpha_{exotic}}}{\alpha_{exotic} + 1} \right] \quad (2.27)$$

If one assumes the dominance of nonexotic contribution both in the s -channel and t -channel, the approximation to the FESR would be reduced to

$$\int_0^N [\text{Im}A_{nonexotic}^{res}]d\nu \sim \left[\beta_{nonexotic} \frac{N^{\alpha_R}}{\alpha_R + 1} \right]. \quad (2.28)$$

Previous authors only considered one duality diagram. In this approximation the FESR relation is not satisfied. Our use of both planar diagrams of Fig. 2.6 have restored the validity of FESR.

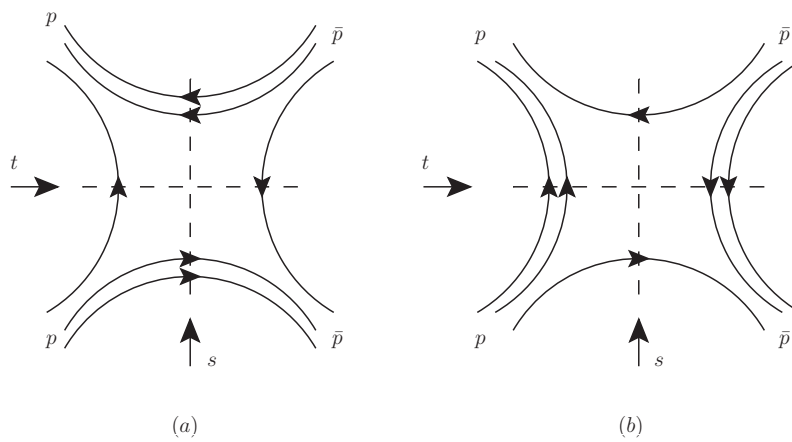


Figure 2.6: A illustration of $\bar{p}p$ s-t channel duality.

Chapter 3

Minijet

In high energy scattering process, the resonance contribution discussed in Chapter 2 is no longer important. The Regge theory alone predicts a constant total cross section at asymptotic energy. However, the nature tells a different story. The total cross sections of all hadronic scatterings rise with energy [1].

In Chapter 1, we mentioned that Cline et al. [2] pointed out that the rise of σ_{pp} can be considered as the same rise as in jet cross section. Phenomenologically, the total cross section is the sum of a soft component, which can be calculated with Regge theory, and a jet cross section, called the hard component, written as

$$\sigma_{tot} = \sigma_{soft} + \sigma_{hard}. \quad (3.1)$$

Experimentally, among the jets produced most of them have relatively small invariant mass, which are referred to as minijets. In the minijet model, the gluon-gluon elastic scattering cross section is used, where a minijet is approximated by a final state gluon with a zero invariant mass. The minijet component is computed using the parton model in pQCD. Nevertheless, the conventional minijet cross section rises too rapidly. In attempt to explain the

data quantitatively, various approaches incorporating eikonal model in minijet have been considered by different authors [21–27].

In this Chapter, we define the conventional QCD-inspired minijet calculation, discuss the problem led by the calculation and present our classical field modified minijet model.

3.1 QCD-inspired minijet

The minijet cross section is defined as the inclusive process in which one counts all the final states that include the specified outgoing jet. It corresponds to the process nucleon A + nucleon B \rightarrow jet + X where X denotes all other particle except the jet. A jet is defined as a cluster of particles, usually mesons, with a small angular distribution. To calculate the minijet cross section, one assumes that the factorization between soft and hard holds for minijet process (The validity of the factorization theorem involving two nucleons in the initial state has been established, although it had been subjected of controversy. [8]) and write the minijet cross section as

$$\sigma_{mnj} = \sum_{a,b=\{q,\bar{q},g\}} \int_{\frac{2\hat{t}_0}{s}}^1 dx_1 \int_{\frac{2\hat{t}_0}{x_1 s}}^1 dx_2 \int_{-\hat{s}+\hat{t}_0}^{-\hat{t}_0} d\hat{t} f_a(x_1, Q^2) f_b(x_2, Q^2) \frac{d\sigma_{ab}}{d\hat{t}}(\hat{s}, \hat{t}), \quad (3.2)$$

where the quantities \hat{s} , \hat{t} and \hat{u} are the Mandelstam variables of the subprocess and $f_a(x, Q^2)dx$ is the number of parton of type a with longitudinal momentum fractions in the interval x to $x + dx$ coming from one of the colliding nucleons in a transverse area of $\delta S = 1/Q^2$. In other words, it is the number of gluon

can be seen by a probe with a trasverse size $1/Q^2$. The momentum scale is usually set as the characteristic momentum transfer of the parton-parton elastic scattering diagram, for example $Q^2 = |\hat{t}|$ for \hat{t} -channel gluon exchange diagram. $f_a(x, Q^2)$ is called the parton distribution function (pdf). $\frac{d\sigma_{ab}}{dt}$ is the differential cross section of the parton-parton elastic scattering. There is a momentum cutoff parameter \hat{t}_0 below which pQCD is not valid and those process with squared momentum transfer smaller than \hat{t}_0 should be included in the soft component instead. Physically, it means in every subprocess there is one parton coming from each nucleon. The two colliding partons undergo elastic scattering, then radiate and produce jets while they are flying away from the scattering center. The minijet cross section is the incoherent sum of the elastic cross section of all binary pairs of the colliding partons.

At very large s , the lower limits of the x_1 - and x_2 -integration in eq. (3.2) reach to a very small value. In small- x region, gluon pdf dominates over all other type of partons (see Fig. 3.1). Therefore, the asymptotic behavior of minijet cross section could be well approximated by considering only gluon contribution as

$$\sigma_{mnj} = \int_{\frac{2\hat{t}_0}{s}}^1 dx_1 \int_{\frac{2\hat{t}_0}{x_1 s}}^1 dx_2 \int_{-\hat{s}+\hat{t}_0}^{-\hat{t}_0} dt g(x_1)g(x_2)F_{mnj} \frac{d\sigma_{gg}}{dt}. \quad (3.3)$$

We introduce the factor F_{mnj} in the definition. For conventional minijet model, $F_{mnj} = 1$. The value of F_{mnj} will be modified as we incorporate classical field effect in the model discussed in Chapter 5. $g(x)$ is the gluon distribution function of the incident nucleons. In general $g(x)$ is a function of x and Q^2 ,

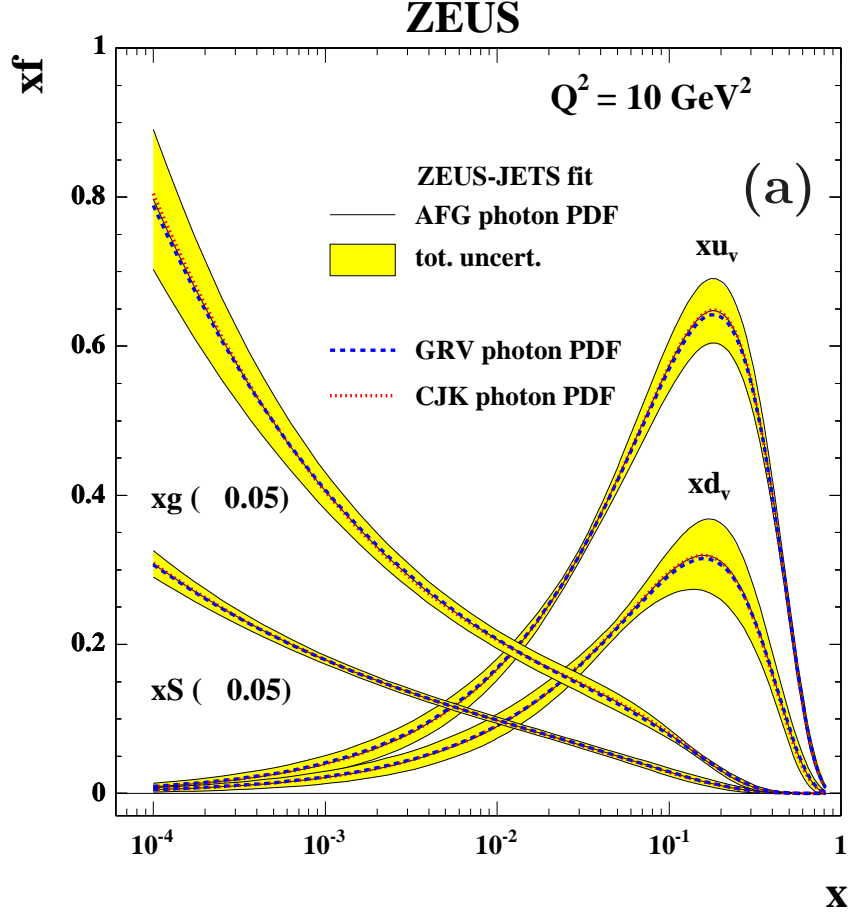


Figure 3.1: ZEUS result [5] of various pdf at $Q^2 = 10 \text{ GeV}^2$. Note that the gluon and sea quark pdfs in the plot are only 5% of their actual values.

where Q^2 can be set to be $|\hat{t}|$ or $|\hat{u}|$, representing the typical momentum scale of the subprocess. Since the differential cross section is singular in both \hat{t} and \hat{u} , we use the peak approximation and set $g(x) = g(x, \hat{t}_0)$, where $\hat{t}_0 = 1 \text{ GeV}^2$ is taken to be the initial value where the gluon evolution starts (DGLAP equation [28–30]). The differential cross section of the gluon-gluon elastic scattering to

the lowest order in pQCD is given by

$$\frac{d\sigma_{gg}}{d\hat{t}} = \frac{\pi\alpha_s^2}{\hat{s}^2}|M|^2, \quad (3.4)$$

where

$$|M|^2 = \frac{9}{2} \left(3 - \frac{\hat{u}\hat{t}}{\hat{s}^2} - \frac{\hat{s}\hat{t}}{\hat{u}^2} - \frac{\hat{u}\hat{s}}{\hat{t}^2} \right) \quad (3.5)$$

$$\approx \frac{9}{2} \left(-\frac{\hat{s}\hat{t}}{\hat{u}^2} - \frac{\hat{u}\hat{s}}{\hat{t}^2} \right). \quad (3.6)$$

For large s , the dominant contributions of the gg subprocess are from the terms with \hat{t} and \hat{u} singularities. The corresponding leading order diagrams are the one gluon exchange diagrams in \hat{t} - and \hat{u} -channel which lead to the final approximation in eq. (3.6). Fig. 3.2 shows this approximation has the same asymptotic behavior as the full calculation up to a normalization.

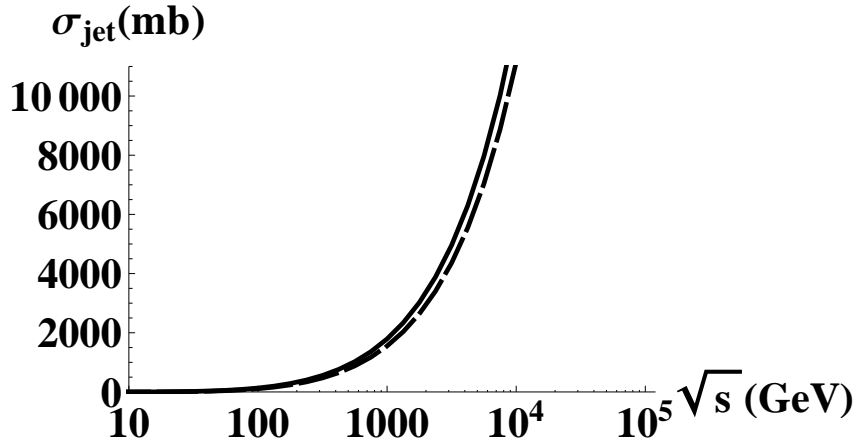


Figure 3.2: Comparison between the mini-jet cross section calculated with the full gg elastic differential cross section (solid line) and that calculated with the last two terms in (3.6) (dashed line).

3.2 Violation of Froissart bound

The integral in eq. (3.3) is dominated by small- x region since $g(x)$ has the conventional parametric form $g(x) \sim x^{-J}$ when x is small [5, 31, 32]. By integrating x_2 and \hat{t} , it leads to the asymptotic form of the integral of x_1 as

$$\begin{aligned} \sigma_{mnj}(s) &= \int_{2\hat{t}_0/s}^1 dx_1 I(x_1, s) \\ &\xrightarrow{s \rightarrow \infty} \frac{1}{\hat{t}_0} \int_{2\hat{t}_0/s}^1 dx_1 \frac{1}{x_1} \left[\left(\frac{s}{2\hat{t}_0} \right)^{J-1} - x_1^{1-J} \right]. \end{aligned}$$

The integration over x_1 leads to

$$\sigma_{mnj}(s) \rightarrow \frac{1}{\hat{t}_0} \left(\frac{s}{\hat{t}_0} \right)^{J-1} \ln \frac{s}{\hat{t}_0}. \quad (3.7)$$

According to the deep inelastic scattering data from HERA and ZEUS, $J \sim 1.3$ [5, 31, 32]. So, at large s , $\sigma_{mnj} \propto s^{0.3} \ln s$ violates Froissart bound [12, 13], which requires $\sigma \leq \text{const.} \times (\ln s)^2$.

3.3 Taming the rise

Many authors have noticed that the minijet cross section rise too rapidly. The first modification is done by Gaißer and Halzen [22]. They found that, in order to fit the data, the momentum cutoff in the minijet integration has to increase as s increases. Another common approach to tame the rise is to use eikonal model [23, 24]. In eikonal model, one uses the diffractive scattering formulation which is consistent with the unitarity constraints and approximates the total cross section by

$$\sigma_{tot} = 4\pi \int_0^\infty db b [1 - e^{-\chi(b,s)}], \quad (3.8)$$

where the eikonal function $\chi(b, s)$ is given by the sum of soft and hard contributions as

$$\chi(b, s) = \frac{1}{2}(A_{soft}(b)\sigma_{soft}(s) + A_{hard}(b)\sigma_{mnj}(s)). \quad (3.9)$$

Each contribution is a product of the cross section and a impact parameter profile function $A(b)$ which satisfies

$$2\pi \int_0^\infty db b A(b) = 1. \quad (3.10)$$

If we consider χ is small and expand the exponential in eq. (3.8), the total cross section reduces to the form given in eq. (3.1). Only when the minijet cross section rises, the higher order terms with alternating sign in the expansion become important and the taming occurs.

The authors of [25] observed that, even with the eikonal model, a fixed momentum cutoff is inadequate. In particular, with the cutoff fixed e.g. at ~ 1 GeV, they found that the minijet cross section in the eikonal model, as in the case of the original minijet model, continues to rise too rapidly with s . They then turned their attention to the effect due to soft gluon emissions. They found that soft gluon emissions could generate an appropriate s -dependence in the impact parameter profile function $A(b, s)$ that leads to agreement with the data [25, 27]. Despite the success of fitting the data with these approaches, eikonal models do not have a firm theoretical foundation (Section 2.4 of [33]).

The use of eikonal model and the consideration of the soft gluon radiation successfully tame the rise of cross section. The eikonal model can be

considered as an effective theory for multiple scattering, while the soft gluon radiation is a non-perturbative ingredient. Those modifications indicate that it is important to incorporate non-perturbative features in the hard component. For this reason, our goal is to formulate an effective correction, which does not depend on the eikonal model, to the minijet calculation.

3.4 Minijet in classical color field

The gluon distribution function rises as $x^{-\lambda}$ when x is small for a fixed Q^2 (see Fig. 3.1). If we consider an external probe with momentum Q^2 , for example the virtual photon in deep inelastic scattering and the exchange gluon in nucleon-nucleon scattering, within the transverse area $1/Q^2$ of the probe, the gluons are dilute when x is large. On the other hand, when x decreases, the gluons become crowded, start to overlap and saturate the vision of the probe. Fig. 3.3 shows the gluon with x inside a nucleon as probed by Q^2 . The big circle is the nucleon and the small circles are the gluons. The size of the gluon seen by the probe with Q^2 is $\sim 1/Q^2$. The dash line divides the saturated region and the dilute region. In the saturated region, gluons overlap on each other. When the probe tries to interact with the constituents, the shadowing effect cannot be ignored. Furthermore, the transition between dilute and saturated gluons introduces a saturation scale $Q_s^2(x) \propto \alpha_s x g(x, Q_s^2) / \pi R^2$ for which being larger than Q^2 , the nucleon is saturated. (See [34] for review.)

In the minijet model at high energy, the contribution to the total cross section is dominated by the small- x gluons. As they are highly shadowed,

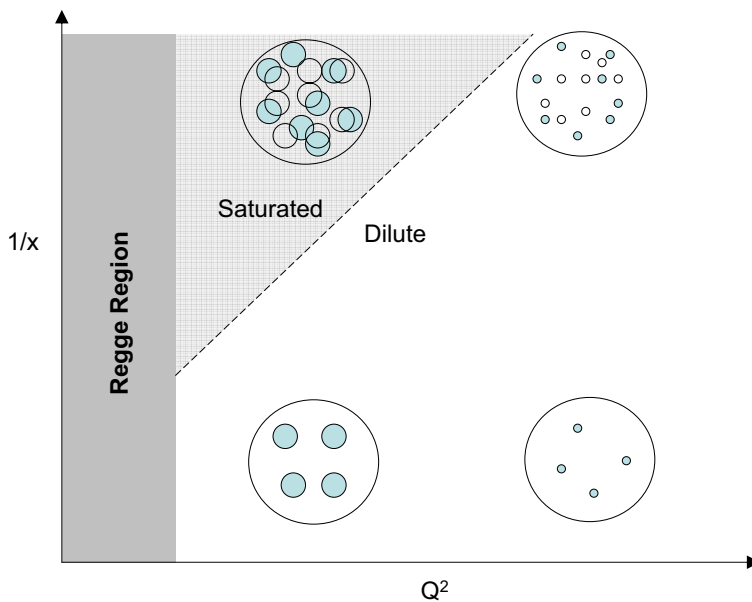


Figure 3.3: A picture of a nucleon in the $\frac{1}{x} - Q^2$ plane.

the saturation effect should be incorporated into the calculation. We consider the following picture. In the center of mass frame, the colliding nucleons are approximately moving at the speed of light. Consider a subprocess of gluon-gluon elastic scattering. To the first order perturbation, the gluons from different nucleons interact by exchanging a gluon with momentum $Q^2 > \Lambda_{QCD}^2$. From the point of view of one of the nucleon, this exchange gluon serves as a probe and strikes one of the constituent gluons with longitudinal momentum fraction x inside this nucleon. When the exchange gluon propagates inside the nucleon, it is also influenced by the other gluons which provide the shadowing

effect. This shadowing would have a typical momentum at Q_s^2 . One expects the minijet model with the correct physics should have the features that

1. if $Q_s^2 < Q^2$, then the exchange gluon sees a dilute nucleon, and the shadowing can be ignored and it reduces to the conventional minijet model; and
2. if $Q_s^2 > Q^2 > \Lambda_{QCD}^2$, then the shadowing is important and the minijet cross section will be suppressed.

To include the shadowing effect, we apply the MV model [35–37]. We assume that the constituent gluons which do not directly interact with the exchange gluon will indirectly involve in the hard scattering as they are treated as a static classical source. The gluons with a smaller x -value is originally radiated by those with larger x via bremsstrahlung in the quantum mechanical framework. In this classical picture, these smaller- x radiation is considered as the classical color field generated by the classical source with a larger- x according to the classical Yang-Mills equation of motion. The presence of the classical field be thought of as a perturbative correction of the vacuum when the source is weak. The hard scattering Feynman diagrams of the two constituent gluons exchanging a gluon will then receive modification due to the non-zero vacuum. All the gluon propagator in the diagram will be modified. However, assuming factorization theorem, those correction on the external gluon propagators can be absorbed in the definition of the initial gluon distribution function and the final fragmentation function. Only the propagator

of the exchange gluon is modified explicitly. This modification leads to the introduction of the modification factor in the minijet cross section formula in eq. (3.3). This modification factor provides suppression to the minijet contributed by the gluon in the saturated region. In the following chapters, we will demonstrate how this factor is derived.

Chapter 4

Classical Effective Theory of Small- x Gluons

4.1 Why does $g(x, Q^2)$ rise?

In the section, we discuss the origin of the rise of small- x gluon distribution. The distribution $g(x, Q^2)$ is characterized by two variables, x and Q^2 , which, in the infinite momentum frame (IMF), represent the longitudinal momentum fraction of the gluon and the momentum scale of the external particle interacting with the nucleon (the probe), respectively. Let us discuss a simplified version of pQCD to illustrate the rise. In strong interaction, the emission of gluons with the smaller x value are favorable through bremsstrahlung. According to pQCD, the probability of emitting a small- x gluon with momentum $(k_\perp, k_z = xP_z)$, where P_z is the momentum of the parent gluon which has a distribution of $g(x = 1, Q^2)$, is given by

$$dP_{Bremsstrahlung} = \frac{\alpha_s N_c}{\pi^2} \frac{d^2 k_\perp}{k_\perp^2} \frac{dx}{x}, \quad (4.1)$$

where $N_c = 3$ for $SU(N_c = 3)$ QCD¹. The evolution when x is fixed and $Q^2 \rightarrow \infty$ is referred to as the Bjorken limit. This dynamics can be well

¹The gluon-to-gluon splitting function is $P_{gg}(x) = 6 \left[\frac{1}{x} - 2 + x(1-x) \right] + \left(\frac{11}{2} - \frac{N_f}{3} \right) \delta(1-x) + 6 \left(\frac{1}{1-x} - \delta(1-x) \int_0^1 dx' \frac{1}{1-x'} \right)$. For small x , it is proportional to $1/x$. If the parent emitter is a quark instead of a gluon, there will not be $1/x$ enhancement.

described by DGLAP evolution equation [28–30]. As at another limit that Q^2 is fixed and $x \rightarrow 0$, the parent gluon can cascade with n intermediate gluon ordered in x . For the n -th cascade, one has

$$\alpha_s^n \int_x^1 \frac{dx_n}{x_n} \int_{x_n}^1 \frac{dx_{n-1}}{x_{n-1}} \dots \int_{x_2}^1 \frac{dx_1}{x_1} = \frac{1}{n!} \left(\alpha_s \ln \frac{1}{x} \right)^n. \quad (4.2)$$

Although, each cascade is suppressed by a factor of α_s , the bremsstrahlung correction is still large as x is small, $\alpha_s \ln 1/x \gtrsim 1$. Therefore, the nucleon is populated by a large amount of low- x gluons. If one ignores the k^2 dependence, summing over all cascade in eq. (4.2) gives the gluon a form of

$$xg(x, Q^2) \sim e^{\alpha_s C \ln(1/x)} = x^{-\alpha_s C}, \quad (4.3)$$

where C is some positive constant.

A formal calculation for this cascade which sums over all the leading $\ln 1/x$ and retain the full Q^2 dependence is referred to as the BFKL equation [38, 39]:

$$-x \frac{\partial}{\partial x} f(x, Q^2) = \frac{3\alpha_s(Q^2)}{\pi} Q^2 \int \frac{d^2 k}{k^2} \left\{ \frac{f(x, k^2) - f(x, Q^2)}{|k^2 - Q^2|} + \frac{f(x, Q^2)}{\sqrt{4k^4 + Q^4}} \right\}, \quad (4.4)$$

where $f(x, Q^2) = \frac{\partial xg(x, Q^2)}{\partial \ln Q^2}$ is the nonintegrated gluon distribution. If one fixes the coupling constant at α_{s_0} , the BKFL equation can be solve analytically and for small- x it gives

$$xg(x, Q^2) \sim \frac{x^{1-\alpha_P}}{\sqrt{\ln(1/x)}}, \quad (4.5)$$

where $\alpha_P = 1 + 12\alpha_{s_0} \ln(2)/\pi$ is referred to as the intercept of the bare QCD pomeron. It confirms the rapid rise of gluon distribution in small- x region.

4.2 Space-time structure of partons

In the infinite momentum frame (IMF), the life time of the partons (gluon or quark) with momentum k in the light-cone coordinate² is $\Delta x^+ \sim \frac{1}{k^-} = \frac{k^+}{k_{\perp}^2} \propto x$. The large- x fast partons survive for a much longer time than the slow small- x gluons. Thus, as far as the dynamics of the slow gluons is concerned, one can treat the fast partons as a static colour source which generates the color field at small x . Although, due to color neutrality assumption, the global color charge average of the fast partons should be zero, the local fluctuation of the source can give a non-zero color charge density. In our approach, the fast partons can be the quarks or gluons with large x .

4.3 Classical field of a nucleon

In this section, we will follow the general assumptions in [34–37, 40] and study the effective theory for the small- x gluons inside a fast moving nucleon.

Consider a nucleon moving along the positive light-cone ($+z$ direction) with velocity $v^{\mu} = (1, 0, 0, 1)$. The charge distribution along the longitudinal direction is Lorentz contracted, while the transverse distribution is given by $\rho(x_{\perp})$. With the static assumption of the source, the source is independent of light-cone time x^+ ,

$$J^{a\mu}(x^-, x_{\perp}) = \delta^{\mu+} \rho^a(x^-, x_{\perp}). \quad (4.6)$$

²See Appendix A.

In Yang-Mills equation, the current is covariantly conserved satisfying

$$[D_\mu, J^\mu] = [D_+, J^+] = \partial_+ J^+ - ig[A_+, J^+] = 0 \quad (4.7)$$

For a non-zero field A^- , the source J^+ will be subjected to color precession. That means if the source at some $x^+ = x_0^+$ is $J^+(x_0^+, x^-, x_\perp)$, the source at other x^+ is given by

$$J^+(x^+, x^-, x_\perp) = V(x^+, x^-, x_\perp) J^+(x_0^+, x^-, x_\perp) V^\dagger(x^+, x^-, x_\perp), \quad (4.8)$$

where V is the Wilson line:

$$V(x^+, x^-, x_\perp) = T \exp \left\{ ig \int_{x_0^+}^{x^+} dz^- A^-(z^+, x^-, x_\perp) \right\}. \quad (4.9)$$

For a static current, $\partial_+ J^+ = 0$, it is consistent to look for solution that satisfies

$$A_+ = A^- = 0. \quad (4.10)$$

The static condition also applies to the field so that A is independent of x^+ , $A^\mu = A^\mu(x^-, x_\perp)$; therefore, the partial derivative of A with respect to x^+ vanishes,

$$\partial_+ A^\mu = \partial^- A^\mu = 0. \quad (4.11)$$

We use the covariant gauge $\partial_\mu A^\mu = 0$ to solve the field equation,

$$D_\nu^{ab} F^{b\mu\nu} = J^{a\mu}. \quad (4.12)$$

The gauge condition together with eq. (4.10) and (4.11) reduces to

$$\begin{aligned} \partial_+ A^+ + \partial_- A^- - \partial_i A_i &= 0 \\ \Rightarrow \partial_i A_i &= 0. \end{aligned} \quad (4.13)$$

Due to the finite size of the nucleon, we use the boundary condition of the field at infinity that $A(|x_\perp| \rightarrow \infty) = 0$. Thus, the gauge condition eq. (4.13) implies

$$A_i(x^-, x_\perp) = 0. \quad (4.14)$$

So only $A^+ = A_-$ is non-zero which also implies $A_\mu^a A^{b\mu} = A^{a-} A^{b+} + A^{a+} A^{b-} - A^{ai} A^{bi} = 0$. These conditions greatly simplify eq. (4.12). The LHS of Eq. (4.12) for $\mu = +$ reduces to

$$D_\nu^{ab} F^{b+\nu} = \partial_\nu F^{a+\nu} + g f^{abc} A_\nu^b F^{c+\nu}$$

The first term is

$$\begin{aligned} \partial_\nu (\partial^+ A^{a\nu} - \partial^\nu A^{a+} + g f^{abc} A^{b+} A^{c\nu}) &= -\square A^{a+} + g f^{abc} (\partial_\nu A^{b+}) A^{c\nu} \\ &= -\square A^{a+} + g f^{abc} (\partial_+ A^{b+}) A^{c+} \\ &= -\square A^{a+}. \end{aligned}$$

For the second term, we have

$$\begin{aligned} g f^{abc} A_\nu^b F^{c+\nu} &= g f^{abc} A_\nu^b (\partial^+ A^{c\nu} - \partial^\nu A^{c+} + g f^{abc} A^{b+} A^{c\nu}) \\ &= g f^{abc} A_-^b (-\partial^- A^{c+} + g f^{abc} A^{b+} A^{c-}) = 0. \end{aligned}$$

Therefore, the field equation becomes

$$\begin{aligned} \square A^{a+}(x^-, x_\perp) &= -\rho(x^-, x_\perp) \\ \Rightarrow (2\partial_+ \partial_- - \partial_i \partial_i) A^{a+}(x^-, x_\perp) &= -\rho(x^-, x_\perp) \\ \Rightarrow \nabla_\perp^2 A^{a+}(x^-, x_\perp) &= \rho(x^-, x_\perp). \end{aligned} \quad (4.15)$$

Eq. (4.15) is the field equation of the classical field for a given source in the covariant gauge with assumptions: (1) the source and the field are static and (2) the field is zero at infinite in the transverse plane. The linearity of the equation validates the fields given by sources moving along the positive light-cone can be obtain by superposition. We write the transverse dependence of ρ^a in momentum space

$$\rho^a(x^-, k_\perp) = \frac{1}{2\pi} \int d^2x_\perp e^{-ik_\perp \cdot x_\perp} \rho^a(x^-, x_\perp), \quad (4.16)$$

for which the solution of the 2D Poisson equation, eq. (4.15) is

$$A_1^{a+}(x^-, x_\perp) = -\frac{1}{(2\pi)^2} \int d^2y_\perp \int d^2k_\perp \frac{\rho_1^a(x^-, y_\perp)}{k_\perp^2} e^{ik_\perp \cdot (x-y)_\perp}. \quad (4.17)$$

We assigns an index 1 to ρ to indicate the source is forward moving. For a source moving toward the opposite direction, the static assumption results $A^+ = 0$ and $\partial^+ A_\mu = 0$. The only non-zero field is

$$A_2^{a-}(x^+, x_\perp) = -\frac{1}{(2\pi)^2} \int d^2y_\perp \int d^2k_\perp \frac{\rho_2^a(x^+, y_\perp)}{k_\perp^2} e^{ik_\perp \cdot (x-y)_\perp}. \quad (4.18)$$

In general, if there are two approaching sources, there will be both non-zero A^+ and A^- . Eq. (4.8) suggests that the sources cannot be treated as static anymore. The field of each source will induce a change in the opposite source. Since we are working toward the first order correction of a bare vacuum due to the source, these cross inductions, which are considered as higher order, will be ignored. Therefore, the total field to the leading order approximation of the source strength is

$$A^{a\mu} = \delta^{\mu+} A_1^{a+}[\rho_1] + \delta^{\mu-} A_2^{a-}[\rho_2] + O(\rho_1\rho_2) + \dots \quad (4.19)$$

This solution in fact is an approximate of eq. (4.12) to first order in ρ_1 and ρ_2 ,

$$\begin{aligned}\partial_\nu F^{a\mu\nu} + g f^{abc} A_\nu^b F^{c\mu\nu} &= V_1 \delta^{\nu+} J_1^{a+} V_1^\dagger + V_2 \delta^{\nu-} J_2^{a-} V_2^\dagger \\ \Rightarrow -\square A^{a\nu} &= \delta^{\nu+} J_1^{a+} + \delta^{\nu-} J_2^{a-}.\end{aligned}$$

Splitting A^ν into $A_1^\nu(x^-, x_\perp) + A_2^\nu(x^+, x_\perp)$, we will have

$$\nabla_\perp^2 A_1^\nu = \delta^{\nu+} J_1^{a+} \quad (4.20)$$

$$\nabla_\perp^2 A_2^\nu = \delta^{\nu-} J_2^{a-} \quad (4.21)$$

which give the solutions in eq. (4.17) and (4.18).

4.4 The McLerran-Venugopalan model

So far the source is not explicitly specified. In fact, it may be impossible to do so, since color objects are confined and only color neutral particle has been observed. However, MV model suggested that the general property of the fluctuation of the source can be specified in the following way.

For simplicity, consider only one nucleon moving along positive light-cone. The source ρ is treated as a random variable. The physical observable O is calculated by first obtaining $O = O[\rho]$ in term of ρ , then averaging over ρ with a Gaussian weight function W written as

$$\begin{aligned}\langle O \rangle_{MV} &= N \int_{\mathcal{D}/\mathcal{G}} \mathcal{D}\rho O[\rho] W[\rho] \\ &= N \int_{\mathcal{D}/\mathcal{G}} \mathcal{D}\rho O[\rho] \exp \left\{ - \int dx^- dx_\perp \frac{(\rho_a(x^-, x_\perp))^2}{2(\lambda(x^-))^2} \right\},\end{aligned} \quad (4.22)$$

where the average is a gaussian integral, N is normalization constant and λ characterizes the correlation between two positions in sources. If two sources are connected by a gauge transformation, the redundancy is excluded in the stochastic average. We denote this domain of the ρ integration as \mathcal{D}/\mathcal{G} .

In QCD, the source will transform if we switch gauge, $\rho \rightarrow U\rho U^\dagger$. The weight function is invariant, as $\rho^a \rho^a = Tr[\hat{\rho}\hat{\rho}]$ and $\mathcal{D}\rho$ is an invariant measure. Therefore, in order to have the observable satisfying gauge invariant, one needs to ensure the observable $O[\rho]$ is also invariant if it is evaluated with a gauge transformed source ρ' such that $O[\rho] = O[\rho']$.

An useful form of the averaging over source configurations is

$$\langle \rho^a(x)\rho^b(y) \rangle_{MV} = \delta^{ab}\delta(x^- - y^-)\delta^2(x_\perp - y_\perp)\lambda(x^-). \quad (4.23)$$

It provides that the total color charge is zero,

$$\langle Q^a \rangle_{MV} = \int dx^- d^2x_\perp \langle \rho^a \rangle = 0, \quad (4.24)$$

and the fluctuation of the charge is non-zero,

$$\begin{aligned} \langle Q^a Q^b \rangle_{MV} &= \int dx^- d^2x_\perp \int dy^- d^2y_\perp \langle \rho^a(x)\rho^b(y) \rangle \\ &= \int dx^- d^2x_\perp \int dy^- d^2y_\perp \delta^{ab}\delta(x^- - y^-)\delta^2(x_\perp - y_\perp)\lambda(x^-) \\ &= \delta^{ab} \int dx^- d^2x_\perp \lambda(x^-) \\ &= \delta^{ab} \int d^2x_\perp \mu, \end{aligned} \quad (4.25)$$

where $\mu = \int dx^- \lambda(x^-)$ is introduced and has the meaning of the average squared color charge of the source in unit of transverse area. This parameter

characterizes the shadowing effect due to saturation. The more the nucleon saturates, the higher the value of μ .

In our calculation, since the field A is linearly dependent on ρ , any non-zero contribution must come from A_1^2 or A_2^2 . The sources from two different nucleons do not correlate; therefore, $\langle A_1[\rho_1]A_2[\rho_2] \rangle = 0$.

Chapter 5

Quantum Gluon Propagator in Classical Field

Equipped with the first order approximation of the classical field of the colliding nucleons, we will formulate a quantum field theory of gluon in the classical field. We will first incorporate the classical field to the QCD Lagrangian with background gauge which is consistent with the covariant gauge when it is applied to the classical field A . By writing the total gauge field as $\mathcal{A} = A + B$, where B is the quantum field, interactions between A and B naturally emerge. We then calculate the leading order correction of the quantum gluon propagator due to the classical field.

5.1 Lagrangian in classical field

In the last chapter we show it is possible to solve for the classical field of two colliding nucleons in the covariant gauge. It has been shown that if one introduces a classical gauge field to the QCD Lagrangian, it is convenient to fix the gauge with background gauge [41]. For the classical field, it requires

$$\bar{D}_\mu^{ab} A^{b\mu} = 0, \tag{5.1}$$

while for the quantum field, we choose the corresponding gauge fixing function to be

$$f^a = \bar{D}_\mu^{ab} B^{b\mu}, \quad (5.2)$$

where where \bar{D} is the covariant derivative involving only A .

$$\bar{D}_\mu^{ac} = (\partial_\mu \delta^{ac} + g f^{abc} A_\mu^b) \quad (5.3)$$

Putting our classical field solution, eq. (4.17) and (4.18) to the LHS of Eq. (5.1), one finds,

$$\begin{aligned} \bar{D}_\mu^{ac} A^{c\mu} &= (\partial_\mu \delta^{ac} + g f^{abc} A_\mu^b) A^{c\mu} \\ &= \partial_\mu (A_1^{a\mu} + A_2^{a\mu}) + g f^{abc} (A_1 + A_2)_\mu^b (A_1 + A_2)^{c\mu} \\ &= g f^{abc} (A_1^{b+} A_2^{c-} + A_1^{c+} A_2^{b-}) \\ &= 0, \end{aligned}$$

the classical field also satisfies background gauge condition.

We write the full Lagrangian, ignoring the fermion field, as the classical QCD Lagrangian with A replaced by $A + B$

$$\mathcal{L}_{QCD} = -\frac{1}{4} F^{a\mu\nu} F_{\mu\nu}^a + J^{a\mu} (A + B)_\mu^a, \quad (5.4)$$

where

$$F^{a\mu\nu} = \partial^\mu (A + B)^{a\nu} - \partial^\nu (A + B)^{a\mu} + g f^{abc} (A + B)^{b\mu} (A + B)^{c\nu}, \quad (5.5)$$

J is the classical source of the nucleons. The Lagrangian is invariant under the infinitesimal gauge transformation,

$$\begin{cases} J^{a\mu} & \rightarrow J'^{a\mu} = (\delta^{ab} - f^{abc} \alpha^c) J^{b\mu} \\ (A + B)_\mu^a & \rightarrow (A' + B')_\mu^a = (A + B)_\mu^a + f^{abc} (A + B)_\mu^b \alpha^c + \frac{1}{g} \partial^\mu \alpha^a \end{cases} \quad (5.6)$$

provided that $\partial_\mu J^\mu = 0$ which is satisfied by a static source. A detail discussion on the gauge invariance of the theory can be found in Appendix B.

5.2 Quantum theory

To formulate a quantum theory for the field B , we assume the only degree of freedom is the field B . The classical field is a prescribed field. We can organize the first term of the Lagrangian in eq. (5.4) in term of the powers of B ,

$$\mathcal{L}_{gauge} \equiv -\frac{1}{4}F^{a\mu\nu}F_{\mu\nu}^a = \mathcal{L}_0 + \mathcal{L}_1 + \mathcal{L}_2 + \mathcal{L}_3 + \mathcal{L}_4 \quad (5.7)$$

where the subscripts represent the order of B containing in each term. \mathcal{L}_0 is independent of B . Upon volume integration it become a constant in the action, so it does not affect the observables and can be ignored. The first order term is

$$\mathcal{L}_1 = -\bar{D}_\nu^{ab} \bar{F}^{b\mu\nu} B_\mu^a + (\text{total derivative}) = -J^{a\mu} B_\mu^a + (\text{total derivative}) \quad (5.8)$$

according to the field equation of the classical field, eq. (4.12), where \bar{F} is the field tensor of A ,

$$\bar{F}^{a\nu\mu} = \partial^\mu A^{a\nu} - \partial^\nu A^{a\mu} + gf^{abc} A^{b\mu} A^{c\nu}. \quad (5.9)$$

This term cancels with $J \cdot B$ in the Lagrangian so that there is no single leg vertex diagram for B . \mathcal{L}_3 and \mathcal{L}_4 contain terms proportional to

$$gB^3, \quad g^2AB^3, \quad g^2B^4.$$

The first type is the original QCD three-gluon vertex. The last two types are higher order terms. Our interest, instead, is in the leading order classical field effect which comes from the quadratic term as

$$\mathcal{L}_2 = \frac{1}{2} B_\mu^a [g^{\mu\nu} \bar{D}_{ac}^\rho \bar{D}_{cb\rho} - \bar{D}_{ac}^\mu \bar{D}_{cb}^\nu - 2g f^{acb} \bar{F}^{c\mu\nu}] B_\nu^b. \quad (5.10)$$

Including the background gauge fixing term

$$\mathcal{L}_{GF} = -\frac{1}{2} (\bar{D}_{ab}^\mu B_\mu^b)^2 = \frac{1}{2} B_\mu^a \bar{D}_{ac}^\mu \bar{D}_{cb}^\nu B_\nu^b + \text{total derivative}, \quad (5.11)$$

the quadratic term in B of the Lagrangian becomes

$$\begin{aligned} \mathcal{L}_2 + \mathcal{L}_{GF} &= \frac{1}{2} B_\mu^a [g^{\mu\nu} \bar{D}_{ac}^\rho \bar{D}_{cb\rho} - 2g f^{acb} \bar{F}^{c\mu\nu}] B_\nu^b \\ &= \frac{1}{2} B_\mu^a [g^{\mu\nu} (\delta^{ab} \square + g f^{acb} (\partial^\rho A_\rho^c + 2A_\rho^c \partial^\rho) \\ &\quad + g^2 f^{aec} f^{cdb} A_\rho^e A^{d\rho}) - 2g f^{acb} \bar{F}^{c\mu\nu}] B_\nu^b \\ &= \frac{1}{2} B_\mu^a [g^{\mu\nu} (\delta^{ab} \square + g f^{acb} 2A_\rho^c \partial^\rho \\ &\quad + g^2 f^{aec} f^{cdb} A_\rho^e A^{d\rho}) - 2g f^{acb} \bar{F}^{c\mu\nu}] B_\nu^b. \end{aligned} \quad (5.12)$$

We can think of the last three terms in eq. (5.12) as interactions between A and B . For example, the term $g g^{\mu\nu} f^{acb} B_\mu^a A_\rho^c \partial^\rho B_\nu^b$ is the vertex with one classical leg and two quantum legs. Since $A = A_1 + A_2$, this term actually represents two types of interactions, one with each nucleon. An interaction with only one power of A does not directly contribute because of the vanishing average $\langle A \rangle = 0$. Therefore, we will expect the gluon to interact with the same classical field through this interaction twice to give a correction at the g^2 order which is the first non-zero order correction. The next term is a vertex with four

legs while two of them are classical. In this term, $A_1 \cdot A_1 = A_2 \cdot A_2 = 0$. It leaves with $g^2 A_1 \cdot A_2$. Again, A_1 and A_2 belongs to two different averaging procedures, $\langle A_1 A_2 \rangle = \langle A_1 \rangle \langle A_2 \rangle = 0$. So we need to have one more interaction with either classical field. However, this term is already at g^2 order. Any extra interaction will give one order higher in g . It will be ignored in our first order calculation. For the last term, we can write the field strength into the sum of field strength due to nucleon 1, F_1 , nucleon 2, F_2 and the cross term F_{12} . Explicitly, the cross term is

$$gF_{12}^{c\mu\nu} = g^2 f^{cde} (A_1^{d\mu} A_2^{e\nu} + A_2^{d\mu} A_1^{e\nu}).$$

The same argument of the vanishing cross term applies also on this case and this cross term can be ignored. The important consequence of having no cross term in the leading order is that the contributions of nucleon 1 and 2 can be calculated independently and additive. Therefore, the final contribution is the sum of the two.

5.3 Propagator

In this section , we will derive the gluon propagator in the field of the nucleon moving to $+z$ direction only. The result can be easily converted to the case of the nucleon moving to $-z$ direction. The propagator of interest is the exchange gluon in the minijet subprocess. It serves as a probe with momentum $q^2 = -Q^2$ of the nucleons or a transverse dimension of the order of $1/Q^2$.

Recall the field of the nucleon has only "+" component and the derivative w.r.t. x^+ vanishes $\partial_+ A^+ = \partial^- A^+ = 0$, so $A_\mu^a A^{b\mu} = 0$ and only the "+i" and "i+" components, $\bar{F}^{a+i} = -\bar{F}^{a+i} = \partial^i A^{a+}$, do not vanish. Eq. (5.12) is simplified to

$$\begin{aligned} \mathcal{L}_2 + \mathcal{L}_{GF} = & \frac{1}{2} B_\mu^a \left[g^{\mu\nu} (\delta^{ab} \square - g f^{abc} 2A^{c+} \partial^-) \right. \\ & \left. + 2g f^{abc} \sum_{i=1}^2 (g^{\mu-} g^{\nu i} - g^{\mu i} g^{\nu-}) \partial_i A^{c+} \right] B_\nu^b. \end{aligned} \quad (5.13)$$

The inverse of the first term gives the Feynman propagator. Let us denote the second term and the third term as

$$\mathcal{L}_{int_1} = -g g^{\mu\nu} f^{abc} B_\mu^a A^{+c} \partial^- B_\nu^b \quad (5.14)$$

$$\mathcal{L}_{int_2} = g f^{abc} \sum_{i=1}^2 B_\mu^a (g^{\mu-} g^{\nu i} - g^{\mu i} g^{\nu-}) \partial_i A^{c+} B_\nu^b \quad (5.15)$$

$$\mathcal{L}_{int} = \mathcal{L}_{int_1} + \mathcal{L}_{int_2} \quad (5.16)$$

There are two kinds of interactions: (1) the gluon changes color but not polarization and (2) the gluon changes both color and polarization. The two-point Green's function to the leading order in $A[\rho]$ is

$$\begin{aligned} & \langle G_{\mu\nu}^{ab}(x, y; \rho) \rangle_{MV} \\ & = \langle T \{ B_\mu^a(x) \left(1 + i \int d^4 z_1 \mathcal{L}_{int}(z_1) \right. \right. \\ & \quad \left. \left. + \frac{i^2}{2!} \int d^4 z_1 d^4 z_2 \mathcal{L}_{int}(z_1) \mathcal{L}_{int}(z_2) \right) B_\nu^b(y) \} \rangle_{MV} \\ & = \langle T \{ B_\mu^a(x) B_\nu^b(y) \} \rangle_{MV} \\ & \quad + \langle T \{ B_\mu^a(x) \frac{i^2}{2!} \int d^4 z_1 d^4 z_2 \mathcal{L}_{int}(z_1) \mathcal{L}_{int}(z_2) B_\nu^b(y) \} \rangle_{MV} \end{aligned}$$

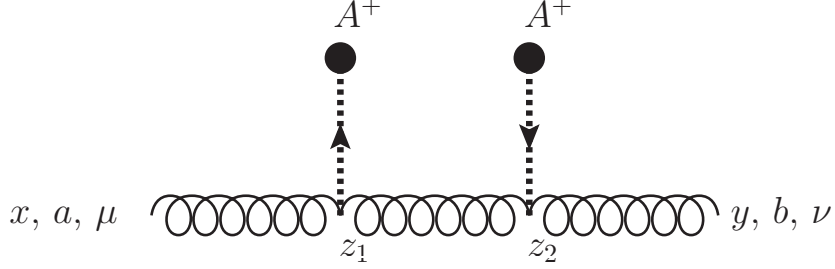


Figure 5.1: Feynman diagram of the propagator in classical field. Each vertex can be \mathcal{L}_{int_1} or \mathcal{L}_{int_2} . The dotted line represents the interaction the momentum exchange between the gluon and the classical field.

where the notation $\langle \dots \rangle_{MV}$ means averaging over classical source defined in eq. (4.22). The interaction term linear in A^+ vanishes because $\langle A^+(x) \rangle_{MV} = 0$. The first term is the Feynman propagator in bare vacuum. The second term represents Feynman diagrams as in Fig. 5.1. There are totally four different contributions coming from the binary pair of interactions \mathcal{L}_{int_1} and \mathcal{L}_{int_2} . We will call them vertex 1 and 2, respectively. and denote the propagator correction involving interactions with two \mathcal{L}_{int_1} as 1-1 term, with two \mathcal{L}_{int_2} as 2-2 term and with the mixed vertices as 1-2 and 2-1 terms.

5.3.1 $\langle A^{a+} A^{b+} \rangle_{MV}$

A crucial ingredient of the calculation is the random source averaging of A . Applying the MV average, eq. (4.23), on $A^{a+} A^{b+}$ of eq. (4.17) gives

$$\langle A^{a+}(z_1) A^{b+}(z_2) \rangle_{MV} = \delta^{ab} \frac{\lambda}{(2\pi)^2} \delta(z_1^- - z_2^-) \int \frac{d^2 k_\perp}{k_\perp^4} e^{i k_\perp \cdot (z_1 - z_2)_\perp}. \quad (5.17)$$

Since we consider the gluon exchange in perturbative region, the gluon propagates only inside the nucleon which is assumed to be an uniformly distributed

source along z^- . The z^- dependence of squared charge density λ is dropped out.

5.3.2 1-1 term

Let us demonstrate the calculation of the propagator due to gluon interacting with \mathcal{L}_{int_1} twice at two positions. Let p_1 , p_2 and p_3 be the momentum of the gluon lines in the left, middle and right, respectively, in Fig. 5.1. The Two-point function is given by

$$\begin{aligned} G_{11}^{+ab}{}_{\mu\nu}(x, y) &= 2 \times \frac{i^2}{2!} \langle T \{ \int d^4 z_1 d^4 z_2 B_\mu^a(x) \mathcal{L}_{int_1}(z_1) \mathcal{L}_{int_1}(z_2) B_\nu^b(y) \} \rangle_{MV} \\ &= - \langle T \{ \int d^4 z_1 d^4 z_2 B_\mu^a(x) (-g f^{cmd} B_\rho^c(z_1) A^{m+}(z_1) \partial^- B^{d\rho}(z_1)) \\ &\quad (-g f^{enf} B_\sigma^e(z_2) A^{n+}(z_2) \partial^- B^{f\sigma}(z_2)) B_\nu^b(y) \} \rangle_{MV} \end{aligned}$$

There are four different ways to contract the fields. The first way is to contract

$$B_\mu^a(x) B_\rho^c(z_1), \quad B^{d\rho}(z_1) B_\sigma^e(z_2), \quad B^{f\sigma}(z_2) B_\nu^b(y),$$

which gives

$$\begin{aligned} G_{11}^{+(1)ab}{}_{\mu\nu}(x, y) &= -g^2 g_{\mu\nu} f^{amd} f^{dnb} \int d^4 z_1 d^4 z_2 \langle A^{m+}(z_1) A^{n+}(z_2) \rangle_{MV} \\ &\quad \frac{d^4 p_1}{(2\pi)^4} \frac{d^4 p_2}{(2\pi)^4} \frac{d^4 p_3}{(2\pi)^4} \frac{-i}{p_1^2} \frac{-i}{p_2^2} \frac{-i}{p_3^2} \\ &\quad e^{-ip_1 \cdot (x-z_1)} (-ip_2^-) e^{-ip_2 \cdot (z_1-z_2)} (-ip_3^-) e^{-ip_3 \cdot (z_2-y)} \end{aligned} \quad (5.18)$$

The MV average of $A^m A^n$ produces δ^{mn} so that $f^{amd} f^{dnb}$ becomes $f^{amd} f^{dmb} = -N_c \delta^{ab}$. In order to carry out the integration of z_1 and z_2 , we write $\langle AA \rangle$ in

4D fourier transform as

$$\langle A^{a+}(z_1)A^{b+}(z_2) \rangle_{MV} = \delta^{ab} \int d^4k_1 d^4k_2 e^{-ik_1 \cdot z_1} e^{-ik_2 \cdot z_2} F(k_1, k_2), \quad (5.19)$$

where

$$F(k_1, k_2) = \frac{\lambda}{(2\pi)^3} \frac{\delta(k_1^-) \delta(k_2^-) \delta(k_{1\perp} + k_{2\perp}) \delta(k_1^+ + k_2^+)}{k_{1\perp}^2 k_{2\perp}^2}. \quad (5.20)$$

With some algebraic manipulations,

$$G_{11}^{+(1)ab}{}_{\mu\nu}(x, y) = -ig^2 g_{\mu\nu} \delta^{ab} N_c (p_2^-)^2 \frac{d^4p_1 d^4p_2 d^4p_3}{(2\pi)^4} \frac{1}{p_1^2 p_2^2 p_3^2} e^{-ip_1 \cdot x + ip_3 \cdot y} F(p_1 - p_2, p_2 - p_3). \quad (5.21)$$

p_2^- and p_3^- combine to be $(p_2^-)^2$ because of the $\delta(k^-) = \delta(p_2^- - p_3^-)$ in F which implies that the classical field does not carry momentum at the $-$ component.

Thus,

$$p_1^- = p_2^- = p_3^-. \quad (5.22)$$

Integrating over p_2 , we have

$$\begin{aligned} I &= \int d^4p_2 \frac{1}{p_2^2 + i\epsilon} F(p_1 - p_2, p_2 - p_3) \\ &= \int d^4p_2 \frac{1}{p_2^2 + i\epsilon} \delta(p_1^- - p_2^-) \delta^4(p_1 - p_3) \frac{\lambda}{(2\pi)^3} \frac{1}{(p_2 - p_1)_\perp^4} \\ &= \delta^4(p_1 - p_3) \frac{\lambda}{(2\pi)^3} \int d^4p_2 \frac{\delta(p_2^- - p_1^-)}{2p_2^+ p_2^- - p_{2\perp}^2 + i\epsilon} \frac{1}{(p_2 - p_1)_\perp^4} \\ &= \delta^4(p_1 - p_3) \frac{\lambda}{(2\pi)^3} \int \frac{dp_2^+}{2p_2^+ p_1^- - p_{2\perp}^2 + i\epsilon} \int \frac{d^2k_\perp}{k_\perp^4} \end{aligned} \quad (5.23)$$

The p_2^+ integration is taken to be the principal value from $-L$ to L as $L \rightarrow \infty$.

$$\int \frac{dp_2^+}{2p_2^+ p_1^- - p_{2\perp}^2 + i\epsilon} = -i\pi \frac{\theta(p_1^-) - \theta(-p_1^-)}{2p_1^-}. \quad (5.24)$$

The origin of the k_{\perp} integration is from integrating the transverse distribution of the classical source ρ . Since the shadowing effect is large for a gluon with a size larger than the probe of Q^2 , $1/k_{\perp}^2 > 1/Q^2$, those gluons are not considered as part of the source. The size of probed source provides an UV-cutoff of the momentum integration of the source k_{\perp} . The IR-cutoff is set to be the QCD scale Λ_{QCD} . Therefore, it becomes

$$\int_{\Lambda_{QCD}^2}^{Q^2} \frac{d^2 k_{\perp}}{k_{\perp}^4} = \frac{\pi(Q^2 - \Lambda_{QCD}^2)}{\Lambda_{QCD}^2 Q^2}. \quad (5.25)$$

The result is

$$G_{11}^{+(1)ab}{}_{\mu\nu}(x, y) = -\frac{g^2 N_c \lambda}{16\pi \Lambda_{QCD}^2} \frac{Q^2 - \Lambda_{QCD}^2}{Q^2} (\theta(q^-) - \theta(-q^-)) g_{\mu\nu} \delta^{ab} \frac{d^4 q}{(2\pi)^4} \frac{q^-}{q^4} e^{-iq \cdot (x-y)}. \quad (5.26)$$

Now we consider the other way to contract the B fields. As we mentioned above, eq. (5.22), that all the “-” components of the momentum are the same. This makes the results of contracting the B fields in the different ways identical. For example, if one contracts $B_{\mu}^a(x)B^{d\rho}(z_1)$ and $B_{\rho}^c(z_1)B_{\sigma}^e(z_2)$. The color index of f^{cmd} becomes f^{dmc} so it picks up a negative sign. However, the ∂^- is now acting on the gluon line with p_1 at z_1 , $\partial^- e^{-ip_1(x-z_1)} = +ip_1^-$. It is different by another negative sign. So there is no overall sign change between the two different contractions. As $p_1^- = p_2^-$, the two contractions become exactly the same. So the contribution due to the 1-1 term is 4 times of the result from any one of the contractions. The propagator correction in momentum space

is given by

$$G_{11}^{+ab}{}_{\mu\nu}(q) = g_{\mu\nu}\delta^{ab} \left(-\frac{g^2 N_c \lambda}{4\pi\Lambda_{QCD}^2} \right) \frac{Q^2 - \Lambda_{QCD}^2}{Q^2} (\theta(q^-) - \theta(-q^-)) \frac{q^-}{q^4}, \quad (5.27)$$

where λ is the squared charge per unit transverse area per unit light-cone longitudinal length the source. The saturation scale Q_s^2 in the color glass condensate framework [34] is defined as

$$\mu = \frac{Q_s^2}{\alpha_s N_c}, \quad (5.28)$$

where $\mu = \lambda L^-$ is the squared charge transverse density and L^- is the longitudinal size of the $+z$ moving source.

5.3.3 1-2 and 2-1 terms

As we have already worked out the 1-1 term, the details for the calculations of the rest of the terms are similar. We will point out a few keys in the calculation. For the 1-2 and 2-1 terms, The interaction term \mathcal{L}_{int_2} consists of a ∂_i on the classical field. In the 1-2 term, \mathcal{L}_{int_1} is at z_1 and \mathcal{L}_{int_2} is at z_2 . The derivative in $\mathcal{L}_{int_2}(z_2)$ acts at position z_2 of $\langle A(z_1)A(z_2) \rangle$ and gives $-ik_\perp$. While the 2-1 term with the same order of contraction will have the derivative acting on z_1 resulting $+ik_\perp$. Each contraction in the 1-2 term will cancel with the that in the 2-1 term.

5.3.4 2-2 term

The interaction vertex is symmetric under exchange of color index $a \leftrightarrow b$ together with Lorentz index $\mu \leftrightarrow \nu$. So there are totally 8 different

contractions, including exchanging z_1 and z_2 , that give identical contributions.

At the level of the Lorentz index, the only surviving term is $\sum_{i,j} -g^{ij} g_\mu^- g_\nu^-$.

The 2-2 term is

$$G_{22}^{+ab}{}_{\mu\nu}(x, y) = i \frac{4g^2 N_c}{(2\pi)^7 \lambda} g_\mu^- g_\nu^- \delta^{ab} \frac{d^4 p_1}{p_1^4} e^{-ip_1 \cdot (x-y)} \int dp_2^+ \frac{1}{2p_2^+ p_1^- p_{2\perp}^2} \int \frac{d^2 k_\perp}{k_\perp^2}. \quad (5.29)$$

$$= i \frac{4g^2 N_c}{(2\pi)^7 \lambda} g_\mu^- g_\nu^- \delta^{ab} \frac{d^4 p_1}{p_1^4} e^{-ip_1 \cdot (x-y)} \frac{-i\pi}{2p_1^-} (\theta(p_1^-) - \theta(-p_1^-)) \int \frac{d^2 k_\perp}{k_\perp^2} \quad (5.30)$$

$$= \frac{4g^2 N_c \pi^2}{(2\pi)^7 \lambda} g_\mu^- g_\nu^- \delta^{ab} \frac{d^4 p_1}{2p_1^- p_1^4} e^{-ip_1 \cdot (x-y)} (\theta(p_1^-) - \theta(-p_1^-)) \ln(Q^2/\Lambda_{QCD}^2) \quad (5.31)$$

Therefore, the propagator correction in momentum space is

$$G_{22}^{+ab}{}_{\mu\nu}(q) = \frac{2g^2 N_c \pi^2 \lambda}{(2\pi)^3} g_\mu^- g_\nu^- \delta^{ab} \frac{\ln(Q^2/\Lambda_{QCD}^2)}{q^- q^4} (\theta(q^-) - \theta(-q^-)) \quad (5.32)$$

5.3.5 Result

We have found the leading order correction of the gluon propagator due to the classical color field in the background gauge. The classical field introduces two type of interactions to the gluon. As for the propagator, single interaction with the classical field does not contribute because of the color neutrality assumption, namely the overall average of color field should be zero. However, the fluctuation can be non-zero so that second order terms contribute. Among all the second order diagrams, only the 1-1 and 2-2 terms survive. The 1-1 term is diagonal in both color and Lorentz structure, while the 2-2 term contains $g_\mu^- g_\nu^-$. When one try to sum a series of 1-1 and 2-2

terms, any series with more than one 2-2 term will be zero. It is because when one connect these diagram with a bare propagator, $g^{\nu\rho}$ is inserted between two diagrams. Therefore, a 2-2 term connecting with a 2-2 term has a form of

$$g_\mu^- g_\nu^- \times g^{\nu\rho} \times g_\rho^- g_\lambda^- = g_\mu^- g^{\rho\rho} g_\lambda^- = 0 \text{ since } g^{\rho\rho} = 0. \quad (5.33)$$

The difference between the nucleons moving in $+z$ and $-z$ is that for the one moving at $-z$ direction, the A field is $A = A^-$ in stead of A^+ . To obtain the interactions, one just needs to exchange the index $+ \leftrightarrow -$ in any fields and derivatives from the interaction term of the $+z$ case. We denote the propagators of the case for $+z$ and $-z$ as G^+ and G^- , respectively.

The classical field modified gluon propagator to the first leading order to the field $A = A_1^+ + A_2^-$ is

$$G_{cl}^{ab}(q) = G_0^{ab}(q) + G_{11}^{+ab}(q) + G_{11}^{-ab}(q) + G_{22}^{+ab}(q) + G_{22}^{-ab}(q), \quad (5.34)$$

where $G_0^{ab}(q) = \frac{-i}{q^2} g_{\mu\nu} \delta^{ab}$ is the bare propagator in vacuum,

$$G_{11}^{\pm ab}(q) = G_0^{ab}(q) \left(i \frac{Q_s^2}{\Lambda_{QCD}^2 L^\mp} \right) \frac{Q^2 - \Lambda_{QCD}^2}{Q^2} \frac{q^\mp}{q^2} (\theta(q^\mp) - \theta(-q^\mp)) \quad (5.35)$$

and

$$G_{22}^{\pm ab}(q) = g_\mu^\mp g_\nu^\mp \delta^{ab} \frac{Q_s^2}{L^\mp} \frac{\ln(Q^2/\Lambda_{QCD}^2)}{q^\mp q^4} (\theta(q^\mp) - \theta(-q^\mp)). \quad (5.36)$$

We have related λ to Q_s^2 using eq. (5.28). Q_s^2 is the saturation scale of the nucleon 1 ($+z$) and 2 ($-z$).

Chapter 6

Implications for Hadronic Cross Sections

In minijet, gluon contribution dominates the cross section at high energy [42]. As discussed in Chapter 3, the minijet cross section rises too rapidly and at high energy gluon density increases to a point that shadowing effect cannot be ignored. We apply the classical field to characterize the shadowing of soft (small- x) gluon field and obtain a correction on the gluon propagator due to the classical field. We are now in the position of applying the modified propagator to minijet model. The underlying idea is that when energy is high and the smaller- x gluon involves in the hard scattering of minijet, one should consider the exchange gluon in the gluon-gluon subprocess is propagating in a field generated by the other gluons in the nucleons, instead of in a vacuum.

6.1 Application to minijet

Let us consider the modification due to nucleon 1, the $+z$ moving nucleon. We use kinematic argument to relate q^- in the modified gluon propagator to q^2 and the energy of the nucleons. Consider, in the center of mass (CM) frame of the collision between two head on nucleons, an exchange gluon is emitted from the nucleon moving to $+z$ direction as in Fig. (6.1). A collinear

gluon from the nucleon with momentum fraction x_1 exchanges a gluon with the gluon in the other nucleon (omitted in the figure). When one applies the propagator to the \hat{t} and \hat{u} channel exchanges, which dominates the minijet cross section (see Chapter 3), the energy-momentum conservation of the vertex and the on-shell condition of the incoming and outgoing gluons requires $q^- = q^2/2x_1P^+$, where $P^+ = \sqrt{s/2}$. Therefore,

$$q^- = \frac{q^2}{x_1\sqrt{2s}}. \quad (6.1)$$

Since $q^2 < 0$ for u and t -channel exchange gluon, so the theta function in eq. (5.35) and (5.36) will give a negative sign. Putting eq. (6.1) into the modified propagator, eq. (5.35) and (5.36) become

$$G_{11}^{+ab}{}_{\mu\nu}(q) = \delta^{ab} g_{\mu\nu} \left(i \frac{Q_s^2}{2\Lambda_{QCD}^2(x_1P^+L^-)} \right) \frac{Q^2 - \Lambda_{QCD}^2}{Q^2} \frac{-i}{q^2}, \quad (6.2)$$

and

$$G_{22}^{+ab}{}_{\mu\nu}(q) = g_\mu^- g_\nu^- \delta^{ab} \frac{\ln(Q^2/\Lambda_{QCD}^2)}{L^-} \frac{Q_s^2}{Q^2} \frac{x_1\sqrt{2s}}{q^4}. \quad (6.3)$$

Further simplification between P^+ and L^- can be made. We define the typical

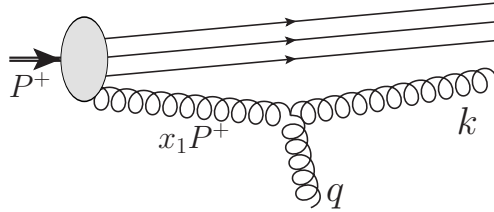


Figure 6.1: Momentum conservation of the vertex and on-shell condition for the incoming(x_1P^+) and outgoing(k) gluons: $-2x_1P \cdot q + q^2 = 0 \Rightarrow q^- = q^2/(2x_1P^+)$.

size of each individual gluon source with longitudinal momentum $x_1 P^+$ to be

$$L^- = \frac{\chi}{x_1 P^+}, \quad (6.4)$$

where χ is a fitted parameter of the order of unity. The value $\chi = 1.34$ is used in our fit to the pp and $\bar{p}p$ data.

For the nucleon going to $-z$, q^+ appears in the correction terms instead of q^- . Looking at the vertex of the exchange gluon in this nucleon, one finds $q^+ = -q^2/(x_2\sqrt{2s})$. So q^+ and q^- have opposite signs. If $q^- > 0$, the contribution from $+z$ moving nucleon pick up the $q^-\theta(q^-) > 0$ in G_{11}^+ and $\theta(q^-)/q^- > 0$ in G_{22}^+ , while $q^+ < 0$ and the contribution of the other hadron comes from $q^+(-\theta(-q^+)) > 0$ in G_{11}^- and $-\theta(-q^+)/q^+ > 0$ in G_{22}^- . The effects from both nucleons always have the same sign and, therefore, their contributions are additive. Combining the two, we arrive at

$$G_{11}^{ab}{}_{\mu\nu}(q) = \delta^{ab} g_{\mu\nu} \left(i \frac{Q_s^2(x_1) + Q_s^2(x_2)}{2\Lambda_{QCD}^2 \chi} \right) \frac{Q^2 - \Lambda_{QCD}^2 - i}{Q^2} \frac{1}{q^2}, \quad (6.5)$$

and

$$G_{22}^{ab}{}_{\mu\nu}(q) = g_\mu^- g_\nu^- \delta^{ab} \frac{\ln(Q^2/\Lambda_{QCD}^2)}{\chi} \frac{x_1^2 Q_s^2(x_1) + x_2^2 Q_s^2(x_2)}{Q^2} \frac{s}{q^4}. \quad (6.6)$$

where x_1 and x_2 are the momentum fractions of the constituent gluons from the nucleons moving to $+z$ and $-z$, respectively.

6.2 Analytic continuation

Fig. 3.3 illustrates the kinematic domain between saturated and dilute region. In the dilute region, pQCD is applicable. But in the saturated region,

even the coupling α_s is small, pQCD does not work well because of the high gluon density. One cannot simply treat the hard scattering as it is under pure vacuum.

The $gg \rightarrow gg$ amplitude in the classical fields can be calculated by replacing the bare propagator of the exchange gluon by the classical field modified propagator. The amplitude is proportional to $G_{\mu\nu}^{cab}(q)$ in eq. (5.34). If one assumes that the amplitude is an analytic function of both Q^2 and $z \equiv \frac{Q_{s1}^2 + Q_{s2}^2}{Q^2}$, $\mathcal{A}(Q^2, z)$ except at one isolated point, at the region where Q^2 is large and z is small, the amplitude should reduce to the result calculated by pQCD and weak classical field method, therefore our result of the amplitude. For $z = 0$, it corresponds to pure pQCD case. On the other hand, one can find an expansion of the amplitude about $z = 0$ for a fixed large Q^2 , then find the corresponding analytic function which is defined in the complex plane of z and has the same expansion for $z \sim 0$. This analytic function of the amplitude analytically continues to the domain that z is large. Therefore, the amplitude in the saturation domain can be constructed by the amplitude in the dilute region using pQCD and weak classical field method.

It is well known that the variables Q_s^2 determine the applicability of pQCD due to asymptotic freedom. We will now explain how z determines the weak classical field so that analytic continuation from small z to large z , in fact, corresponds to going from dilute to saturated region. For simplicity, let consider only on nucleon, therefore, fix x_2 . z can be thought of as $z = Q_s^2/Q^2$ (We suppress the subscribe 1 in Q_s^2). Since Q_s^2 is proportional to the squared

charge density μ of the source, it is proportional also to the number of particles (gluons), N , inside the nucleon of size R_N . On the other hand, the exchange gluon has a transverse size of $R_Q = 1/Q^2$. One can define $N_Q = R_N/R_Q$ as the number of probe can be fitted in a nucleon. If we define a "saturated" region to be where, on average, having at least one particle in each probe which can be fitted in the nucleon. If the ratio

$$\frac{N}{N_Q} < 1, \text{ it is dilute;}$$

$$\frac{N}{N_Q} > 1, \text{ it is saturated.}$$

Writing the ratio in term of Q^2 and Q_s^2 ,

$$\frac{N}{N_Q} \propto \frac{Q_s^2}{R_N/R_Q} = \frac{Q_s^2}{Q^2 R_N} \propto \frac{Q_s^2}{Q^2 R_N}$$

Therefore, indeed, the variable $z = Q_s^2/Q^2$ characterizes the saturated/dilute property of the nucleon.

We want to find out the leading contribution to the amplitude, therefore the propagator, at the dilute region. For fixed (x_1, x_2) and $x_1 > x_2$, (suppressing the color and Lorentz index)

$$G_{11} \propto \frac{z}{\Lambda_{QCD}^2} \left(1 - \frac{\Lambda_{QCD}^2}{Q^2} \right), \quad (6.7)$$

$$G_{22} = \frac{\ln(Q^2/\Lambda_{QCD}^2) x_1^2 Q_s^2(x_1) + x_2^2 Q_s^2(x_2)}{\chi} \frac{s}{Q^2} \frac{1}{q^4} \quad (6.8)$$

$$< \frac{\ln(Q^2/\Lambda_{QCD}^2) Q_s^2(x_1) + Q_s^2(x_2) x_1^2 s}{\chi} \frac{1}{Q^2} \frac{1}{q^4} \quad (6.9)$$

$$\propto \ln(Q^2/\Lambda_{QCD}^2) z \frac{x_1^2 s}{Q^4} \quad (6.10)$$

For a large enough Q^2 , $G_{11} \rightarrow \frac{z}{\Lambda_{QCD}^2}$ and $G_{22} \rightarrow 0$. So the leading order correction in z is $G_{11} \sim \frac{z}{\Lambda_{QCD}^2}$ in the pQCD and weak field domain. Together with the bare propagator, it is

$$G^{cl}(Q^2 = -q^2, z) = g_{\mu\nu}\delta^{ab}\frac{-i}{q^2} + g_{\mu\nu}\delta^{ab}\frac{-i}{q^2}(izCq^2), \quad (6.11)$$

where

$$C = \frac{1}{2\chi\Lambda_{QCD}^2}. \quad (6.12)$$

6.3 Resummation

Now we start to analytically continue eq. (6.11) from large Q^2 and $z \approx 0$ to other z value for a fixed Q^2 by finding the analytic function of the propagator as a function of z of which the first order Taylor expression at $z = 0$ matches the our pQCD result. To do this, we take eq. (6.11) and use the fact that $\frac{1}{1-z} \approx 1 + z + \dots$,

$$G^{cl}(Q^2 = -q^2, z) = g_{\mu\nu}\delta^{ab}\frac{-i}{q^2}(1 + (izCq^2)) \quad (6.13)$$

$$\rightarrow g_{\mu\nu}\delta^{ab}\frac{-i}{q^2}\frac{1}{1 - (izCq^2)} \quad (6.14)$$

$$= g_{\mu\nu}\delta^{ab}\frac{-i}{q^2}\frac{1}{1 + iC(Q_s^2(x_1) + Q_s^2(x_2))}. \quad (6.15)$$

Eq. (6.15) is analytic for the entire complex plane of z except at $z = -i/(Cq^2)$. Therefore, by analytic continuation, this expression of the modified propagator is valid for all value of z , including the saturated region where $z > 1$. This result corresponds to summing over a series of the diagrams with n -number

of elements $g_{\mu\nu}\delta^{ab}\frac{-i}{q^2}(izCq^2)$. Diagrammatically, it corresponds to the series in Fig. 6.2. Each blob represents the gluon's interaction with the A field from

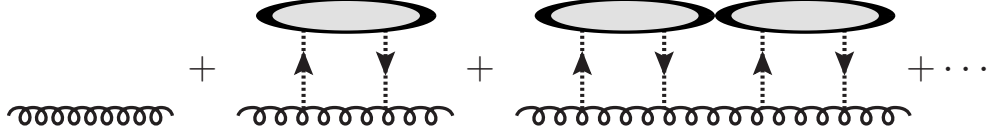


Figure 6.2: Schematic Feynman diagram which represents the iterative sum of the modified propagator. The first term is the bare propagator. The blob and the two lines connecting to it in the series represent the interaction between the quantum gluon propagator and the classical field.

both hadrons and contributes the same multiplicative factor. The sum of the series is simply a geometric sum. So the final form of the propagator is the product of the bare propagator and a correction factor,

$$f = \frac{1}{1 + iC(Q_s^2(x_1) + Q_s^2(x_2))} \quad (6.16)$$

as eq. (6.15).

6.4 Modification factor in Minijet

Upon taking an absolute square of the $gg \rightarrow gg$ amplitude of gluon exchange diagram, a new factor

$$F_{mnj}^{cl} \equiv |f|^2 = \frac{1}{1 + C^2(Q_s^2(x_1) + Q_s^2(x_2))^2} \quad (6.17)$$

is introduced to the minijet cross section of the dominating \hat{t} - and \hat{u} -channel diagrams. We refer to F_{mnj}^{cl} as the classical field modification factor which is a function of x_1 and x_2 . If both x_1 and x_2 are large, $F_{mnj}^{cl}(x_1, x_2)$ is close

to unity. When one of the x , x_1 or x_2 , becomes small, F_{mnj}^{cl} is less than 1. Therefore, the contribution from the region where either x_1 or x_2 is small is suppressed. For example, when x_2 is large and x_1 is small, then $F_{mnj}^{cl}(x_1 \ll 1, x_2 \sim 1) \rightarrow 1/(1 + C^2 Q_s^2(x_1)^2)$. In both cases, the minijet cross section can still be considered as factorisable. However, in the region where both x_1 and x_2 are small, both $Q_s^2(x_1)$ and $Q_s^2(x_2)$ are large. Their contributions are important, as these contributions that make dependence on x_1 and x_2 in the minijet calculation non-factorisable. The behavior of F_{mnj}^{cl} is illustrated in Fig. 6.3, where we used the parameterization of Q_s^2 discussed in the next section.

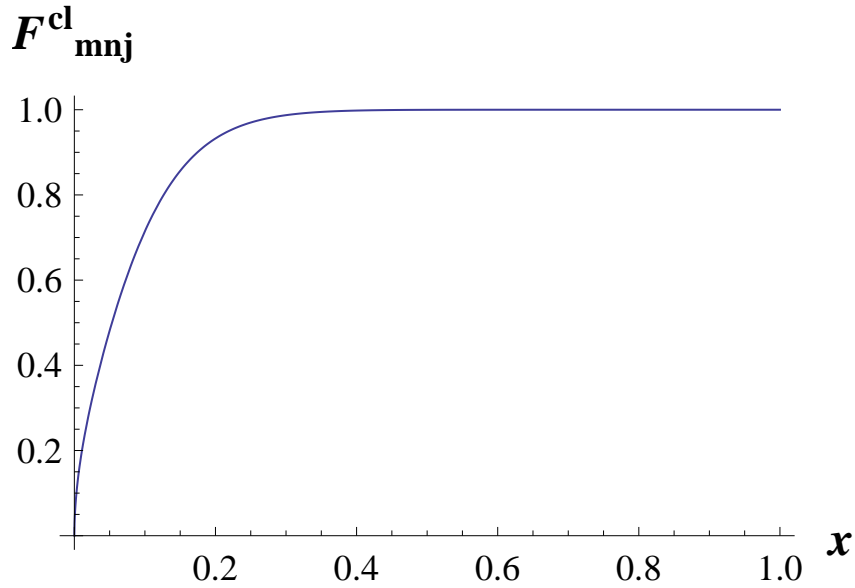


Figure 6.3: x_1 -dependence of F_{mnj}^{cl} while keeping $x_2 = 1$

Chapter 7

Result and Discussion

7.1 pp and $\bar{p}p$ total cross section at high energy from modified minijet model

We recall that the minijet cross section is dominated by the \hat{t} - and \hat{u} -channel contributions and for those diagrams the modified propagator introduced a modification factor to the integral of the minijet cross section. We have

$$\sigma_{mnj}^{cl}(s) = \int_{\frac{2i_0}{s}}^1 dx_1 \int_{\frac{2i_0}{x_1 s}}^1 dx_2 \int_{-\hat{s}+t_0}^{-t_0} d\hat{t} g(x_1)g(x_2) \frac{d\sigma'}{d\hat{t}} F_{mnj}^{cl}(x_1, x_2) \quad (7.1)$$

where

$$F_{mnj}^{cl}(x_1, x_2) = \frac{4\chi^2 \Lambda_{QCD}^4}{4\chi^2 \Lambda_{QCD}^4 + (Q_s^2(x_1) + Q_s^2(x_2))^2}, \quad (7.2)$$

and $d\sigma'/d\hat{t}$ is the sum of the singular terms in \hat{t} and \hat{u} in eq. (3.6). We take the QCD scale $\Lambda_{QCD} = 0.2$ GeV and a fixed coupling constant¹ $\alpha_s = 0.33$. We follow the parametrization of $g(x)$ in [44] and write

$$g(x, Q_0^2 = 1 \text{ GeV}^2) = 1.2x^{-1.28}(1-x)^{5.6}. \quad (7.3)$$

¹As shown in Fig. 23 in [43], data points of present interest are following: at $Q \sim 1.5$ GeV, $\alpha_s \sim 0.4$ and at $Q \sim 2.5$ GeV, $\alpha_s \sim 0.3$. The average value is at $Q = 2$ GeV with $\alpha_s \sim 0.33$

The \hat{t} -cutoff is taken to be 1 GeV^2 since $g(x)$ is parametrized starting at $Q_0^2 = 1 \text{ GeV}^2$. For F_{mnj}^{cl} , we take Q_s^2 which is parametrized with a power law in x from the analysis of HERA data [9] as

$$Q_s^2(x) = Q_0^2 \left(\frac{x_0}{x}\right)^\lambda (1-x)^{5.6}, \quad (7.4)$$

with the typical values compatible to earlier analyses [9, 45]:

$$\lambda = 0.28, \quad Q_0^2 = 1 \text{ GeV}^2 \quad \text{and} \quad x_0 = 0.6 \times 10^{-4}. \quad (7.5)$$

The extra factor $(1-x)^{5.6}$ is added to ensure $Q_s^2 \rightarrow 0$ when $x \approx 1$. Since $Q_s^2 \propto xg(x)$, we follow the parameterization of $g(x)$ in eq. (7.3). For the cross section of the soft component, we take

$$\sigma_{soft}^{pp} = \sigma_{soft} \quad (7.6)$$

$$\sigma_{soft}^{\bar{p}p} = \sigma_{soft} \left(1 + \frac{a}{\sqrt{s}}\right), \quad (7.7)$$

where $\sigma_{soft} = 38.5 \text{ mb}$ and $a = 1.5 \text{ GeV}$. We compare the total cross section to the pp and $\bar{p}p$ data for energy $5 \text{ GeV} \leq \sqrt{s} \leq 30 \text{ TeV}$. The results of pp and $\bar{p}p$ total cross sections from the present model are shown in Fig. 7.1 as curves a and b, respectively. Curve e shows the rapid rise of the original minijet cross section. Comparing curves a and b with curve e, one sees there is a strong suppression effect in the present model, which leads to the agreement with the data. In Fig. 7.1, curves c and d are included to illustrate the sensitivity of the value of λ used.

Note that our calculation is intended to show the effect of the modified propagator. We use a fixed coupling constant α_s and $g(x)$ at $Q^2 = \hat{t}_0 = 1$

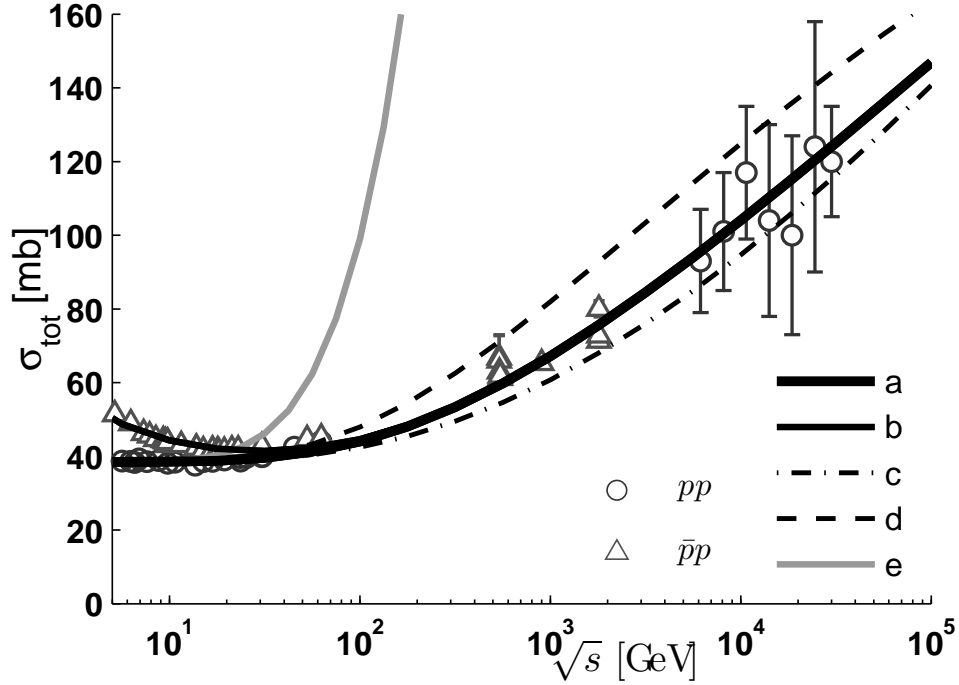


Figure 7.1: Comparison between pp and $\bar{p}p$ data with classical field modified minijet model. Curves a and b are σ_{pp} and $\sigma_{\bar{p}p}$ of the present model where Q_s^2 is defined in eq. (7.4) and (7.5), with $\lambda = 0.28$. Curves c and d are for σ_{pp} with $\lambda = 0.25$ and 0.33 , respectively. Curve e is the original minijet model with $F_{mnj} = 1$. The data is from [1].

GeV^2 . Since the minijet is dominated by the singularities at \hat{t} and \hat{u} , the corresponding Q^2 does not extend beyond the neighborhood of \hat{t}_0 .

7.2 Asymptotic behavior of the σ_{mnj}^{cl} and the $J = 1 + \lambda$ relationship

From eq. (7.1), after integrating over \hat{t} and keeping the leading term in s , the classical field modified minijet cross section is given by $\sigma_{mnj}^{cl} \equiv$

$(9\pi\alpha_s^2/\hat{t}_0)H(J, \lambda, s)$ where

$$H(J, \lambda, s) \propto \int_{\frac{2\hat{t}_0}{s}}^1 dx_1 \int_{\frac{2\hat{t}_0}{x_1 s}}^1 dx_2 \frac{1}{x_1^J x_2^J} \frac{1}{(x_1^{-\lambda} + x_2^{-\lambda})^2}. \quad (7.8)$$

The asymptotic behavior depends mainly on the values of J and λ and can be categorized into three cases. Case (a): For $J < 1 + \lambda$, H approaches to a constant. Case (b): For $J > 1 + \lambda$, H grows as $s^{J-1-\lambda}$. Case (c): $J = 1 + \lambda$

$$H \propto \frac{1}{2\lambda^2} \log \left[\frac{1}{4} \left(\frac{s}{2\hat{t}_0} \right)^\lambda \left[1 + \left(\frac{2\hat{t}_0}{s} \right)^\lambda \right]^2 \right] \\ \xrightarrow{s \rightarrow \infty} \ln (s/2\hat{t}_0) / 2\lambda. \quad (7.9)$$

Among the three cases, case (c) is the only choice for the rising asymptotic behavior of the pp and $\bar{p}p$ cross section that does not violate Froissart bound since it rises as $\ln s$. This choice also implies the identity

$$J = 1 + \lambda. \quad (7.10)$$

We observe that this relationship is consistent with earlier analyses of the data. For example, the value of $J \sim 1.3$ from gluon distribution analysis [44] and the value of $\lambda \sim 0.3$ from geometric scaling [9].

Theoretically, the relation between J and λ of eq. (7.10) could be understood within the MV framework. To see this, consider a fast moving nucleon which consists of gluons with the longitudinal fraction ranging from 0 to 1. Let x be the longitudinal momentum fraction of the gluon which involves in the hard scattering subprocess with some value in between 0 and 1. This gluon, in the context of the MV model, will serve as a division point between

the source and the classical field. Among all gluons, the source gluons have the momentum fraction $x_{source} > x$ and the classical gluon field produced by the source gluons will be associated with $x_{field} < x$. Recall that in the CGC model, $\mu = \frac{Q_s^2}{\alpha_s N_c}$ represents the number density of the source, which, for small- x , is given by $Q_s^2 \propto \int_x^1 dx' g(x') \sim xg(x) \sim x^{1-J}$, assuming gluon source dominates. Matching the powers of x leads to $1 - J = -\lambda$ or eq. (7.10). In our modified minijet model, the power matching is the necessary and sufficient condition for the minijet cross section to satisfy Froissart bound.

7.3 Why is minijet production suppressed in the small x region?

Let us examine the reason why the minijet production is suppressed in the small x region. Notice that the modification factor in eq. (7.2) is suppressive as shown in Fig. 6.3. The smaller x_1 and/or x_2 , the larger the denominator function and the stronger the suppression. It is related to the fact that when the value of x is smaller, which means z is also smaller, the exchange gluon is probing a denser medium. In the saturation region, the classical field is stronger, and in turn the shadowing effect on the propagator gluon is more influential. Thus, the suppression is stronger. This is analogous to the situation in geometric optics. Consider a light ray traversing a darkish medium: the darker the medium, the stronger the absorption of light. For the present case, the interaction between the gluon and the classical field contribute an imaginary part to the correction (See eq. (6.11)). Analogously,

in the geometric optics language, a non-zero imaginary part of the index of refraction means that medium is absorptive.

7.4 Minijet cross section of pA and AA

One of the differences in the present minijet model from the original minijet is the prediction on how the minijet cross section scales with nucleon numbers in nucleon-nucleus (e.g. pA) and nucleus-nucleus (AA) collision at high energy. In the pA case, the original minijet model predicts that the minijet cross section is linear to the total the nucleon number in a nucleus if one natively assumes the parton distribution function (pdf) of a nucleus is A times the pdf of a nucleon.

$$\sigma_{mnj} \propto A. \quad (7.11)$$

In the present model, the pdf is the same so it will also be linear to A . However, the classical field modified factor F_{mnj}^{cl} goes like $1/(Q_s^4)$ for large Q_s^2 . Q_s^2 is proportional the number of gluons per transverse area (recall μ in Chapter 5 and 6), so that $Q_s^2 \propto A/A^{2/3} = A^{1/3}$. Thus, the minijet cross section would have an A dependence as

$$\sigma_{mnj}^{cl} \propto \frac{A}{A^{2/3}} = A^{1/3}. \quad (7.12)$$

Following the same reasoning, for the case of AA, the original minijet predicts

$$\sigma_{mnj} \propto A^2, \quad (7.13)$$

while the present model will have

$$\sigma_{mnj}^{cl} \propto \frac{A^2}{A^{2/3} + A^{2/3}} \propto A^{4/3}. \quad (7.14)$$

Chapter 8

Summary

In this dissertation, we considered one of the unresolved problems in theoretical particle physics, namely how to calculate total cross section in hadron-hadron collision at high energy. In the 60's, physicists studied this problem and predicted that the total cross section would stay constant even for higher collision energy. Intuitively, this conclusion is appealing because hadron is a composited object with a finite geometric size. The cross section should approach to its size. However, as collision energy increases, experiments show the total cross section rises with energy. Therefore, the size of a proton would appear to grow with energy!

In this work, in order to understand the complete picture of the hadronic total cross section from low to high energy, we started with a review on the Regge theory which is a viable theory for small momentum exchange. Duality implies that if there are nonexotic resonances, in the intermediate energy region, the cross section should decrease with energy. Otherwise, the cross section stays constant. From the t -channel point of view, this different energy dependences can be understood in terms of the exchange of exchange-degenerate trajectories. This provides a good reason for the difference between pp and

$\bar{p}p$ cross section at \sqrt{s} lower than 30 GeV. Although Regge theory is not considered as a fundamental theory, it serves as a complementary tool for one to understand the low energy physics.

For the rise of the cross section, we focused on the well accepted theory for strong interaction, the quantum chromodynamics (QCD). In QCD, the fundamental particles are quarks and gluons. Hadrons are bound states and resonances of quarks or antiquarks bounded together by gluons. As a quantum field theory, particles can be created as long as energy allows. For this reason, QCD provides a natural way to explain the rise of the cross section; namely as energy increases more particles can be created inside the hadron, as a result more scatterings can occur. In turn the cross section increases with energy, even though the actual geometric size of the hadron does not. We reviewed the conventional QCD inspired minijet model in Chapter 3 and discussed that the minijet model with the currently accepted gluon distribution function will generate a rapid rise in s with $\sigma \sim s^{0.3} \ln s$ that violates the asymptotic bound of hadronic cross section, the Froissart bound, which only allows $\sigma \leq \text{const} \times (\ln s)^2$. The rapid rise is directly related to the increase of gluon density in the hadron. It is believed that when gluon density is high, simple perturbation (pQCD) will break down even when coupling is small because of multiple scattering or shadowing effect. Treating the dense gluonic medium is important to understand strong interaction at high energy, in general.

In 1994, McLerran and Venugopalan (MV) proposed an effective theory

to describe the high density soft gluons, the small- x gluon, as a classical color field generated by the other large- x constituents in the hadron. As long as the hadron is strongly boosted forward (backward), the large- x partons can be treated as a Lorentz contracted steady classical color source moving along the forward (backward) light-cone. The Yang-Mills equation of the classical field can be solved exactly including the non-linear effect for one single hadron or perturbatively (in our case, to the first order) for two colliding hadrons. Since then this theory has been extensively studied and is referred to as Color Glass Condensate (CGC). In CGC, the key concern is the classical field itself (For review, see [46–48]). The particle production in collision is associated with the field intensity far away from the collision center. Multiplicity of the particle production can be calculated [49–56]. The modified propagator for fermion was also considered [57–62]. So far, the quantitative prediction on the total cross section is not available.

In this work, we took a slightly different path from the CGC. We adopted the point of view of MV to find the classical for to the leading order for two colliding hadrons. Then we formulated a quantum theory for the quantum gluon in the presence of the classical field. The classical field is treated as a prescribed field, instead of a dynamical field, in contrast with CGC. We obtained the classical field modified propagator of the quantum gluon with pQCD to the leading order of coupling constant and leading order of classical field strength in the dilute region. We then analytically continued the result to the saturated domain where shadowing of high density small- x gluons is

important. For consistency check, we derived the condition for gauge invariance of the propagator in the model and showed it was satisfied. The detail is provided in Appendix B.

In Chapter 6, we applied the modified propagator to the minijet model. The modified propagator introduced a modification factor to the minijet cross section. This factor suppresses the contribution from the constituent small- x gluons since they are in the saturation region. As for the large- x gluons, the modified minijet model converges to the conventional minijet model. We calculated the pp and $\bar{p}p$ total cross section and compared it with the data in Chapter 7. We found that the data from $\sqrt{s} = 5$ GeV to 30 TeV can be well described by the sum of a soft and a hard components where the soft component is motivated by Regge theory and the hard component is calculated with our classical field modified minijet model. The modification factor alone provides a correct taming of the rapid rise of the total cross section. More intriguingly, the present model yields a Froissart bound respectful asymptotic behavior with $\sigma \sim \ln s$. We also briefly discussed the extension of the present model to nucleus collisions and explored the nucleon number dependence of the pp , pA and AA total cross section.

To conclude, we integrated the effective classical theory and the quantum theory to formulate a method to treat scattering problem in high energy strong interaction physics. Both the classical and the quantum theories can be directly derived from QCD Lagrangian. The need of both classical and quantum regimes of QCD indicates that strong interaction is non-trivial, yet

interesting that a simple theory could yield and unify different emerging effects. As for the present model, the classical field provides an universal description of different hadrons at high energy. Having nucleon as a reference point, the applicability of model has a potential to be extended to other strongly interacting particles, including mesons, baryon, nucleus and even photon at extremely high energy.

Appendices

Appendix A

Light-cone Coordinate

A 4-vector, p , in the light-cone coordinate is defined in relation to its (0,1,2,3) components as

$$p^+ = \frac{1}{\sqrt{2}}(p^0 + p^3) \quad (\text{A.1})$$

$$p^- = \frac{1}{\sqrt{2}}(p^0 - p^3) \quad (\text{A.2})$$

$$p^1 = p^1 \quad (\text{A.3})$$

$$p^2 = p^2 \quad (\text{A.4})$$

The dot product of a and b is

$$a \cdot b = a^+b^- + a^-b^+ - a^1b^1 - a^2b^2. \quad (\text{A.5})$$

So the absolute square of a vector a^μ is

$$a \cdot a = 2a^+a^- - a^1a^1 - a^2a^2. \quad (\text{A.6})$$

The matrix tensor $g^{\mu\nu}$ is

$$g^{+-} = g^{-+} = g_{+-} = g_{-+} = 1, \quad (\text{A.7})$$

$$g^{ij} = g_{ij} = -\delta^{ij}, \quad (\text{A.8})$$

the other components vanish. As a result,

$$a^+ = a_- \tag{A.9}$$

$$a^- = a_+ \tag{A.10}$$

$$a^i = a_i \tag{A.11}$$

$$\tag{A.12}$$

For a massless particle or a particle approximately moving at the speed of light toward $+z$ direction with energy E , its momentum vector in light-cone coordinate is

$$p^+ = \sqrt{2}E \tag{A.13}$$

$$p^- = 0 \tag{A.14}$$

$$p^i = 0 \tag{A.15}$$

Appendix B

Gauge Invariance

In this Appendix, we will use functional method to derive a gauge invariant condition for the two-point Green's function of the propagator and use it to check gauge invariance. We generalized the Slavnov-Taylor identity [63, 64] to the presence of an non-zero background field.

B.1 Gauge transformation with background

We start with the generating functional

$$\begin{aligned} \mathcal{Z}[\eta; \rho] = & \int \mathcal{D}B \Delta(f(B)) \\ & \times \exp \left\{ i \int d^4x (\mathcal{L}_0(A + B, \rho) + \mathcal{L}_{GF} + \eta_\mu^a B^{a\mu}) \right\} \end{aligned} \quad (\text{B.1})$$

where N is a normalization constant and the gauge fixing function f is chosen as

$$f^a(B) = \bar{D}_\mu^{ab} B^{b\mu} \quad (\text{B.2})$$

such that

$$\mathcal{L}_{GF} = -\frac{1}{2} (\bar{D}_{ab}^\mu B_\mu^b)^2, \quad (\text{B.3})$$

Since the classical field A is chosen to be a prescribed field, it does not transform. As a result, B takes all the burden of the gauge transformation. The

infinitesimal gauge transformation becomes

$$\begin{cases} \rho^{a\mu} & \rightarrow \rho'^{a\mu} = (\delta^{ab} - f^{abc}\alpha^c)\rho^{b\mu} \\ A_\mu^a & \rightarrow A'_\mu^a = A_\mu^a \\ B_\mu^a & \rightarrow B'_\mu^a = B_\mu^a + f^{abc}(A + B)_\mu^b\alpha^c + \frac{1}{g}\partial^\mu\alpha^a \end{cases} \quad (\text{B.4})$$

Hence,

$$\begin{aligned} \frac{\delta f^a(x)}{\delta\alpha^c(y)} &= \bar{D}_\mu^{ab} \frac{\delta B_\mu^b}{\delta\alpha^c(y)} \\ &= \bar{D}_\mu^{ab} \left(f^{bde}(A + B)^{d\mu}\delta^{ec}\delta(x - y) + \frac{1}{g}\partial^\mu\delta^{bc}\delta(x - y) \right) \end{aligned} \quad (\text{B.5})$$

$$= \frac{1}{g}\bar{D}_{x\mu}^{ab} [\partial^\mu\delta^{bc}\delta(x - y) + g f^{bdc}(A_x + B_x)^{d\mu}\delta(x - y)] \quad (\text{B.6})$$

$$\begin{aligned} &= \frac{1}{g} [\delta^{ab}\square\delta(x - y) \\ &\quad + g f^{adc}(2A_{x\mu}^d\partial^\mu + \partial^\mu A_{x\mu}^d + B_{x\mu}^d\partial^\mu + \partial^\mu B_{x\mu}^d)\delta(x - y) \\ &\quad + g^2 f^{aeb} f^{bdc} A_{x\mu}^e (A_x + B_x)^{e\mu}\delta(x - y)]. \end{aligned} \quad (\text{B.7})$$

The subscript x is a abbreviation of the argument of the function, e.g. $A_x = A(x)$. We define

$$M^{ac}(x, y) = \bar{D}_{x\mu}^{ab} [\partial^\mu\delta^{bc}\delta(x - y) + g f^{bdc}(A_x + B_x)^{d\mu}\delta(x - y)] \quad (\text{B.8})$$

with a inverse $M^{-1cd}(x, y)$ satisfying

$$\begin{aligned} &\int dy \bar{D}_{x\mu}^{ab} [\partial^\mu\delta^{bc}\delta(x - y) \\ &\quad + g f^{bdc}(A_x + B_x)^{d\mu}\delta(x - y)] M^{-1cd}(y, z) \\ &= \delta^{ad}\delta(x - z) \end{aligned} \quad (\text{B.9})$$

The determinant of the gauge fixing function with respect to the infinitesimal gauge transformation is

$$\Delta(f) = \det \left(\frac{\delta f^a(x)}{\delta\alpha^b(y)} \right) = \det(M) \det\left(\frac{1}{g}\right). \quad (\text{B.10})$$

The determinant of $1/g$ can be absorbed into the normalization constant N .

This determinant can also be written as a ghost term in the Lagrangian:

$$\begin{aligned} \det(M) = \int \mathcal{D}\bar{c}\mathcal{D}c \exp \left\{ -i \int d^4x [\bar{c}_a \square c_a \right. \\ \left. + g f^{abc} \bar{c}_a (2A_\mu^b \partial^\mu + \partial^\mu A_\mu^b + B_\mu^b \partial^\mu + \partial^\mu B_\mu^b) c_c \right. \\ \left. + g^2 f^{aeb} f^{bdc} \bar{c}_a A_\mu^d (A + B)^{e\mu} c_c \right] \end{aligned} \quad (\text{B.11})$$

Additional interactions between the ghost and the classical field A are also introduced. The connected n -point Green's function of the quantum gluon is given by taking n -derivative with respect to the source η then divided by Z evaluating at $\eta = 0$

$$G_{\mu_1, \mu_2, \dots, \mu_n}^{a_1, a_2, \dots, a_n}(x_1, x_2, \dots, x_n) = \frac{(-i)^n}{Z} \frac{\delta^n Z}{\delta \eta_{a_1}^{\mu_1}(x_1) \dots \delta \eta_{a_n}^{\mu_n}(x_n)} \Bigg|_{\eta=0} \quad (\text{B.12})$$

B.2 Slavnov-Taylor Identity

As we mentioned above, the observable has to be gauge invariant. The transition amplitude depends explicitly on the Green's functions which itself depends on the gauge fixing. Therefore, one need find out a set of conditions on the Green's functions to ensure gauge invariance. This is equivalent to restrict the generating functional to be invariant under gauge transformation. To do that, we transform the generating functional using Eq.(B.4) such that

$$\begin{aligned} \mathcal{Z}[\eta; \rho] \rightarrow \mathcal{Z}'[\eta; \rho'] = N \int \mathcal{D}B' \Delta(f(B')) \\ \exp \left\{ i \int d^4x (\mathcal{L}_0(A + B', rho') + \mathcal{L}_{GF}(B') + \eta_\mu^a B'^{a\mu}) \right\} \end{aligned} \quad (\text{B.13})$$

Since \mathcal{L}_0 is gauge invariant,

$$\mathcal{L}_0(A + B', \rho') = \mathcal{L}_0(A + B, \rho),$$

and the Jacobian of the transformation on $\mathcal{D}B$ is 1,

$$\mathcal{D}B = \mathcal{D}B',$$

the difference between Z and Z' is due to the change in gauge fixing term, the determinant $\Delta(f)$ and the source term ηB .

$$\begin{aligned} Z' &= N \int \mathcal{D}B (\Delta + \delta\Delta) \exp \left\{ i \int d^4x \left(\mathcal{L}_0 + \mathcal{L}_{GF} + \delta\mathcal{L}_{GF} + \eta_\mu^a B^{a\mu} + \eta_\mu^a \delta B^{a\mu} \right) \right\} \\ &\sim N \int \mathcal{D}B \Delta \left(1 + \frac{\delta\Delta}{\Delta} \right) \left[1 + i \int d^4x \left(\delta\mathcal{L}_{GF} + \eta_\mu^a \delta B^{a\mu} \right) \right] \\ &\quad \times \exp \left\{ i \int d^4x \left(\mathcal{L}_0 + \mathcal{L}_{GF} + \eta_\mu^a B^{a\mu} \right) \right\} \\ &= Z + N \int \mathcal{D}B \Delta \left[\frac{\delta\Delta}{\Delta} + i \int d^4x \left(\delta\mathcal{L}_{GF} + \eta_\mu^a \delta B^{a\mu} \right) \right] \\ &\quad \times e \left\{ i \int d^4x \left(\mathcal{L}_0 + \mathcal{L}_{GF} + \eta_\mu^a B^{a\mu} \right) \right\}. \end{aligned} \tag{B.14}$$

We require that

$$\begin{aligned} 0 = \delta Z &= N \int \mathcal{D}B \Delta \left[\frac{\delta\Delta}{\Delta} + i \int d^4x \left(\delta\mathcal{L}_{GF} + \eta_\mu^a \delta B^{a\mu} \right) \right] \\ &\quad \times e \left\{ i \int d^4x \left(\mathcal{L}_0 + \mathcal{L}_{GF} + \eta_\mu^a B^{a\mu} \right) \right\} \end{aligned} \tag{B.15}$$

for all $\alpha^a(x)$.

$$\begin{aligned}
\delta\mathcal{L}_{GF} &= -\frac{1}{2}2f^a\delta f^a \\
&= -(\bar{D}_\mu^{ab}B^{b\mu})(\bar{D}_\mu^{ab}\delta B^{b\mu}) \\
&= -(\bar{D}_\mu^{ab}B^{b\mu})\bar{D}_\mu^{ab}\left(f^{cde}(A+B)^{d\mu}\alpha^e + \frac{1}{g}\partial^\mu\alpha^c\right) \\
&= -(\bar{D}_\mu^{ab}B^{b\mu})\frac{1}{g}\int dy M^{ac}(x,y)\alpha^c(y)
\end{aligned} \tag{B.16}$$

where M is defined in Eq.(B.8)

$$\begin{aligned}
\eta_\mu^a\delta B^{a\mu} &= \eta_\mu^a\left[f^{ade}(A+B)_x^{d\mu}\alpha^e(x) + \frac{1}{g}\partial^\mu\alpha^a(x)\right] \\
&= \eta_\mu^a f^{adc}(A+B)_x^{d\mu}\alpha^c(x) - \frac{1}{g}(\partial^\mu\eta_\mu^a)\alpha^a(x) + \frac{1}{g}\partial^\mu(\eta_\mu^a\alpha^a) \\
&= \left[\eta_\mu^a f^{adc}(A+B)_x^{d\mu} - \frac{1}{g}(\partial^\mu\eta_\mu^a)\delta^{ac}\right]\alpha^c(x) + \frac{1}{g}\partial^\mu(\eta_\mu^a\alpha^a)
\end{aligned} \tag{B.17}$$

From here on we will denote $\Delta(f)$ as the determinant of $M^{ab}(x,y)/g$. After the transformation, M becomes $M + \delta M$ and the determinant becomes, under gauge transformation (B.4),

$$\begin{aligned}
\Delta' &= \det(M + \delta M) = \det(\bar{D}_{x\mu}^{ab}[\partial^\mu\delta^{bc}\delta(x-y) + gf^{bdc}(A_x + B'_x)^{d\mu}\delta(x-y)]) \\
&= \det(\bar{D}_{x\mu}^{ab}[\partial^\mu\delta^{bc}\delta(x-y) + gf^{bdc}(A_x + B_x)^{d\mu}\delta(x-y) \\
&\quad + gf^{bdc}f^{dmn}(A_x + B_x)^{m\mu}\alpha_x^n\delta(x-y) \\
&\quad + f^{bdc}(\partial_x^\mu\alpha_x^d)\delta(x-y)])
\end{aligned}$$

Expanding Δ' to first order in δM

$$\begin{aligned}
\Delta' &= \det(1/g) \det(M + \delta M) \\
&= \det(1/g) \det(M) \det(1 + \delta M M^{-1}) \\
&= \det(1/g) \det(M) \exp(\text{Tr} \log(1 + \delta M M^{-1})) \\
&\sim \det(1/g) \det(M) \exp(\text{Tr}[\delta M M^{-1}]) \\
&\sim \det(1/g) \det(M) (1 + \text{Tr}[\delta M M^{-1}]) \\
&= \det(1/g) \Delta (1 + \text{Tr}[\delta M M^{-1}]).
\end{aligned}$$

One can identify

$$\frac{\delta \Delta}{\Delta} = \text{Tr}(\delta M M^{-1}).$$

Explicitly M and δM reads

$$\begin{aligned}
M_x^{ac} \phi^c(x) &= \bar{D}_{x\mu}^{ab} [\partial^\mu \delta^{bc} \phi^c + g f^{bdc} (A_x + B_x)^{d\mu} \phi^c] \\
\delta M^{ac} \phi^c &= \bar{D}_{x\mu}^{ab} [g f^{bdc} f^{dmn} (A_x + B_x)^{m\mu} \alpha_x^n \phi^c + f^{bdc} (\partial_x^\mu \alpha_x^d) \phi^c],
\end{aligned}$$

therefore, the trace becomes¹

$$\begin{aligned}
Tr[\delta M M^{-1}] &= Tr [\bar{D}_{x\mu}^{ab} [g f^{bcd} f^{dmn} (A_x + B_x)^{m\mu} \alpha_x^n M^{-1ce}(x, y) \\
&\quad + f^{bcd} (\partial_x^\mu \alpha_x^d) M^{-1ce}(x, y)]] \\
&= \int dx dy \bar{D}_{x\mu}^{ab} [g f^{bcd} f^{dmn} (A_x + B_x)^{m\mu} \alpha_x^n M^{-1ce}(x, y) \\
&\quad + f^{bcd} (\partial_x^\mu \alpha_x^d) M^{-1ce}(x, y)] \delta^{ae} \delta(x - y) \\
&= \int dx [g f^{akl} f^{lcn} (\partial_x^\mu A_{x\mu}^k M^{-1ca}(x, x)) \\
&\quad + g^2 f^{akl} f^{lde} f^{dmn} A_{x\mu}^k (A + B)_x^{m\mu} M^{-1ca}(x, x)] \alpha_x^n
\end{aligned} \tag{B.18}$$

The total contribution from eq.(B.16), (B.17) and (B.18) to the deviation of Z is, neglecting the total derivative term,

$$\begin{aligned}
&\frac{\delta \Delta}{\Delta} + i \int d^4x \left(\delta \mathcal{L}_{GF} + \eta_\mu^a \delta B^{a\mu} \right) \\
&= \int dx [g f^{akl} f^{lcn} (\partial_x^\mu A_{x\mu}^k M^{-1ca}(x, x)) \\
&\quad + g^2 f^{akl} f^{lde} f^{dmn} A_{x\mu}^k (A + B)_x^{m\mu} M^{-1ca}(x, x)] \alpha_x^n \\
&\quad - \int dx dy (\bar{D}_\mu^{ab} B^{b\mu}) \frac{1}{g} M^{ac}(x, y) \alpha^c(y) \\
&\quad + \int dy \left[\eta_\mu^a f^{adc} (A + B)_y^{d\mu} - \frac{1}{g} (\partial^\mu \eta_\mu^a) \delta^{ac} \right] \alpha^c(y)
\end{aligned}$$

Let an arbitrary function

$$\chi_x^a = M_x^{ab} \alpha_x^b \tag{B.19}$$

¹ $Tr[f(x, y)] = \int dx dy \delta(x - y) f(x, y) = \int dx f(x, x)$

Therefore,

$$\begin{aligned}
& \frac{\delta\Delta}{\Delta} + i \int d^4x \left(\delta\mathcal{L}_{GF} + \eta_\mu^a \delta B^{a\mu} \right) \\
&= \int dx dy \left[g f^{akl} f^{lcn} (\partial_x^\mu A_{x\mu}^k M^{-1ca}(x, x)) \right. \\
&\quad \left. + g^2 f^{akl} f^{ldc} f^{dmn} A_{x\mu}^k (A + B)_x^{m\mu} M^{-1ca}(x, x) \right] M^{-1ne}(x, y) \chi^e(y) \\
&\quad - \int dy \left(\bar{D}_\mu^{eb} B^{b\mu}(y) \right) \frac{1}{g} \chi^e(y) \\
&\quad + \int dx dy \left[\eta_\mu^a f^{adc} (A + B)_x^{d\mu} - \frac{1}{g} (\partial^\mu \eta_\mu^a) \delta^{ac} \right] M^{-1ce}(x, y) \chi^e(y)
\end{aligned}$$

The generalized Slavnov-Taylor identity is given by the equation

$$\begin{aligned}
\delta Z = 0 = & \left\{ \int dx \left[g f^{akl} f^{lcn} (\partial_x^\mu A_{x\mu}^k M^{-1ca}(x, x)) M^{-1ne}(x, y) \right. \right. \\
& \left. \left. + g^2 f^{akl} f^{ldc} f^{dmn} A_{x\mu}^k (A + B)_x^{m\mu} M^{-1ca}(x, x) \right] M^{-1ne}(x, y) \right. \\
& \left. - \frac{1}{g} \bar{D}_\mu^{eb} B_y^{b\mu} \right. \\
& \left. + \int dx \left[\eta_\mu^a f^{adc} (A + B)_x^{d\mu} - \frac{1}{g} (\partial^\mu \eta_\mu^a) \delta^{ac} \right] M^{-1ce}(x, y) \right\} \mathcal{Z}
\end{aligned} \tag{B.20}$$

The equation is an abbreviation of

$$\{ \dots \} \mathcal{Z} = \int \mathcal{D}B \{ \dots \} e^{i \int dx \mathcal{L}_0 + \mathcal{L}_{GF} + \eta B}$$

To the leading order, the first two terms in eq. (B.20) are neglected because they are at least one g order higher than the last two. Differentiating the last two terms with respect to $\eta_\nu^c(z)$ and setting all $\eta = 0$, we obtain

$$\begin{aligned}
0 = & \left\{ \bar{D}_{\mu y}^{eb} B_y^{b\mu} B_z^{c\nu} \right. \\
& \left. + i \left[g f^{cdb} (A + B)_z^{d\nu} + \partial^\nu \delta^{cb} \right] M_{be}^{-1}(z, y) \right\} \mathcal{Z} \Big|_{\eta=0}
\end{aligned} \tag{B.21}$$

By taking a covariant derivative $\bar{D}_{z\nu}^{e'c}$, the second term becomes delta functions according to eq. (B.8) leading to

$$\left\{ \bar{D}_{\mu y}^{eb} \bar{D}_{\nu z}^{dc} B_y^{b\mu} B_z^{c\nu} + i\delta^{ed}\delta(z-y) \right\} \mathcal{Z}|_{\eta=0} = 0 \quad (\text{B.22})$$

By identifying the connected two-point Green's function as

$$G_{\mu\nu}^{bc}(x, y) = \frac{1}{\mathcal{Z}} \{ B_x^{b\mu} B_y^{c\nu} \} \mathcal{Z}|_{\eta=0}$$

and taking the MV average of eq. (B.22), it leads to

$$\langle \bar{D}_x^{ac\mu} \bar{D}_y^{bd\nu} G_{\mu\nu}^{cd}(x, y; \rho) \rangle_{MV} = -i\delta^{ab}\delta^4(x-y) \quad (\text{B.23})$$

This condition is analogous to the transversality condition of gluon Green's function in Slavnov's original derivation (eq. (22) and (23) in [63]). One can check the propagator derived in Section 5 satisfies eq. (B.23)

B.3 Gauge invariance of the modified propagator

We will show the green's function to the leading order in g and A^2 satisfies the generalized Slavnov-Taylor identity, eq. (B.23). For simplicity, only one nucleon will be considered. Since the contributions of the cross terms involving two colliding source vanished after the MV average, the proof can be easily generalized to the two nucleons case.

In eq. (B.23), the MV average is taken after acting the covariant derivative on the Green's function (GF). The covariant derivative consists of a linear term in A which multiplying with the first order term in A of the GF will have

non-zero contribution. Therefore, besides the terms we calculated in Section 5, one needs to calculate the diagram that has only one interaction with the classical field.

Firstly, we argue that the interaction term

$$\mathcal{L}_{int_2} = gf^{abc} \sum_i B_\mu^1 (g^{\mu-} g^{\nu i} - g^{\mu i} g^{\nu-}) \partial_i A^{c+} B_\nu^b$$

should be considered as of order A^2 for the following reason. An similar argument can be found in [65]. In the MV average, the volume integration of $\langle \rho \rho \rangle$ is the density of the source in a volume $L^- L_\perp^2$, where L^- is the size of the source along the light-cone – direction and L_\perp^2 is the transverse size of the source. Recall eq. (4.23)

$$\langle \rho^a(x) \rho^b(y) \rangle_{MV} = \delta^{ab} \delta(x^- - y^-) \delta^2(x_\perp - y_\perp) \frac{\mu}{L^-}. \quad (\text{B.24})$$

Integrating both sides of eq. (B.24) over a volume gives

$$\int \langle \rho \rho \rangle_{MV} dV \sim \frac{\mu}{L^-}, \quad (\text{B.25})$$

where the LHS is has a dimension of $1/\text{Volume} = 1/(L^- L_\perp^2)$. We defines a typical transverse correlated size L_\perp of two local sources as

$$L_\perp \sim \frac{1}{\sqrt{\mu}}. \quad (\text{B.26})$$

Eq. (B.25) also implies $\rho \sim \sqrt{\frac{\mu}{L_\perp^2 L^-}} = \frac{\sqrt{\mu}}{L^- L_\perp}$. Eq. (5.17) suggests that A^2 is proportional to $\mu/((L^-)^2 \Lambda_{QCD}^2) \sim \mu$ both L^- and Λ_{QCD} are related to the

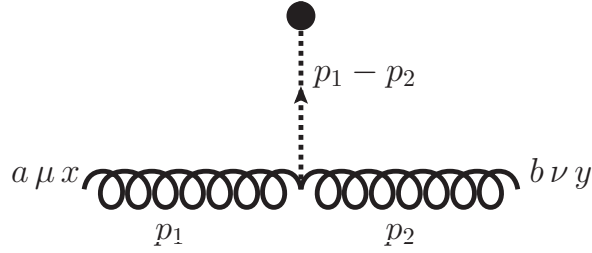


Figure B.1: Schematic Feynman diagram for gluon GF with single interaction with A .

confinement scale. Therefore, the transverse derivative in \mathcal{L}_{int_2} is of the order of

$$\partial_{\perp} A \sim \frac{A}{L_{\perp}} \sim \sqrt{\mu} \sqrt{\mu} = \mu \sim A^2.$$

For this, we conclude \mathcal{L}_{int_2} is of the order of $O(A^2)$, although it is only explicitly linear in A . Thus, the diagram which has two vertices of \mathcal{L}_{int_2} is considered as a higher order, $O(A^4)$, contribution and will not be included in the checking of gauge invariance.

B.3.1 Terms linear in \mathcal{L}_{int_1} and \mathcal{L}_{int_2}

We have calculated the terms of $O(A^2)$ in Section 5. To check gauge invariant, we also need the other terms that vanish only after taking the MV average. There are two of these term. One is from \mathcal{L}_{int_1} and the other from \mathcal{L}_{int_2} . Diagrammatically, we consider a gluon enter from the left with momentum p_1 then interacts at z and leaving with momentum p_2 as shown in Fig. (B.1)

For the first term with vertex of \mathcal{L}_{int_1} , the GF is

$$G_{\mu\nu}^{Iab}(x, y) = i \langle T B_\mu^a(x) \int dz \mathcal{L}_{int_1}(z) B_\nu^b(y) \rangle \quad (\text{B.27})$$

$$= i(-g) f^{cmd} \int dz \langle T B_\mu^a(x) g^{\alpha\beta} B_\alpha^c(z) A^{c+} \partial^- B_\beta^d(z) B_\nu^b(y) \rangle. \quad (\text{B.28})$$

There are two way to contract the fields. The sum of the two contributions is

$$G_{\mu\nu}^{Iab}(x, y) = g g_{\mu\nu} f^{abc} \int d^4 z \frac{d^4 p_1 d^4 p_2 (p_1^- + p_2^-)}{(2\pi)^8 p_1^2 p_2^2} A^{c+}(z) e^{-ip_1(x-z) - ip_2(z-y)} \quad (\text{B.29})$$

The second term comes from the interaction with \mathcal{L}_{int_2} and is given by

$$G_{\mu\nu}^{IIab}(x, y) = -2g f^{abc} (g_\mu^- g_\nu^i - g_\mu^i g_\nu^-) \quad (\text{B.30})$$

$$\int \frac{d^4 p_1 d^4 p_2 \partial_i A^{c+}(z) d^4 z}{(2\pi)^8 p_1^2 p_2^2} e^{-ip_1(x-z) - ip_2(z-y)}. \quad (\text{B.31})$$

However, this term does not contribute to eq. (B.4) to $O(A^2)$ because it is explicitly linear to A which will vanish after taking MV average. On the other hand, when we multiple the A in the covariant derivative to this term, its contribution is non-zero, but it excesses the order of A^2 .

B.3.2 Checking gauge invariant

Let us rewrite the LHS of eq. (B.23) according to the order of A as

$$\begin{aligned} & \langle \bar{D}_x^{ac\mu} \bar{D}_y^{bd\nu} G_{\mu\nu}^{ab}(x, y) \rangle_{MV} \\ &= \langle \partial_x^\mu \partial_y^\nu G_{0\mu\nu}^{ab}(x, y) \rangle_{MV} \quad (O(1)) \\ &+ \langle \partial_x^\mu g f^{bcd} A^{c\nu}(y) G_{\mu\nu}^{Iad}(x, y) + \partial_y^\nu g f^{acd} A^{c\nu}(x) G_{\mu\nu}^{Idb}(x, y) \rangle_{MV} \quad (O(A^2)) \\ &+ \langle \partial_x^\mu \partial_y^\nu G_{11\mu\nu}^{+ab}(x, y) \rangle_{MV} \quad (O(A^2)). \end{aligned}$$

The $O(1)$ term is the derivatives on a bare Feynman propagator. The MV average provide no effect to this term. Straight forward evaluation gives

$$\begin{aligned}
& \delta^{ab} g_{\mu\nu} \partial_x^\mu \partial_y^\nu \int \frac{d^4 q}{(2\pi)^4} \frac{-i}{q^2} e^{-iq(x-y)} \\
&= \delta^{ab} \int \frac{d^4 q}{(2\pi)^4} (-i) e^{-iq(x-y)} \\
&= -i \delta^{ab} \delta(x-y),
\end{aligned}$$

which is the RHS of eq. (B.23).

The first term of the $O(A^2)$ term is

$$\begin{aligned}
& \langle \partial_x^\mu g f^{bcd} A^{c\nu}(y) G_{\mu\nu}^{Iad}(x, y) \rangle \\
&= \langle \partial_x^\mu g f^{bcd} A^{c\nu}(y) g g_{\mu\nu} f^{ade} \int d^4 z \frac{d^4 p_1 d^4 p_2}{(2\pi)^8} \frac{(p_1^- + p_2^-)}{p_1^2 p_2^2} A^{e+}(z) e^{-ip_1(x-z) - ip_2(z-y)} \rangle_{MV} \\
&= g^2 f^{bcd} f^{ade} \langle A^{c+}(y) A^{e+}(z) \rangle_{MV} \partial_x^- \int d^4 z \frac{d^4 p_1 d^4 p_2}{(2\pi)^8} \frac{(p_1^- + p_2^-)}{p_1^2 p_2^2} e^{-ip_1(x-z) - ip_2(z-y)}.
\end{aligned}$$

Using eq. (5.19), we have

$$\begin{aligned}
& \langle \partial_x^\mu g f^{bcd} A^{c\nu}(y) G_{\mu\nu}^{Iad}(x, y) \rangle \\
&= -N_c g^2 \delta^{ab} \int d^4 k_1 d^4 k_2 F(k_1, k_2) (-ip_1^-) \int d^4 z \frac{d^4 p_1 d^4 p_2}{(2\pi)^8} \frac{(p_1^- + p_2^-)}{p_1^2 p_2^2} \\
&\quad \times e^{-i(p_1+k_1)x} e^{i(p_1-k_2-p_2)z} e^{ip_2 y} \\
&= -N_c g^2 \delta^{ab} \int d^4 k_1 d^4 k_2 F(k_1, k_2) (-ip_1^-) \frac{d^4 p_1 d^4 p_2}{(2\pi)^8} \frac{(p_1^- + p_2^-)}{p_1^2 p_2^2} \\
&\quad \times e^{-i(p_1+k_1)x} (2\pi)^4 \delta^4(p_1 - k_2 - p_2) e^{ip_2 y} \\
&= i N_c g^2 \delta^{ab} \int d^4 k_1 F(k_1, p_1 - p_2) (p_1^-) \frac{d^4 p_1 d^4 p_2}{(2\pi)^4} \frac{(p_1^- + p_2^-)}{p_1^2 p_2^2} e^{-i(p_1+k_1)x} e^{ip_2 y} \\
&= i N_c g^2 \delta^{ab} \int d^4 k_1 \frac{\lambda}{(2\pi)^3} \delta^4(k_1 + (p_1 - p_2)) \frac{\delta(k_{1\perp}^-)}{k_{1\perp}^4} (p_1^-) \\
&\quad \times \frac{d^4 p_1 d^4 p_2}{(2\pi)^4} \frac{(p_1^- + p_2^-)}{p_1^2 p_2^2} e^{-i(p_1+k_1)x} e^{ip_2 y} \\
&= \delta^{ab} i \frac{N_c g^2 \lambda}{(2\pi)^7} \int d^4 p_1 d^4 p_2 \frac{\delta(p_1^- - p_2^-)}{(p_1 - p_2)_\perp^4} (p_1^-) \frac{(p_1^- + p_2^-)}{p_1^2 p_2^2} e^{-i(p_1 - (p_1 - p_2))x} e^{ip_2 y} \\
&= \delta^{ab} i \frac{2N_c g^2 \lambda}{(2\pi)^7} \int d^4 p_1 d^4 p_2 \frac{\delta(p_1^- - p_2^-)}{(p_1 - p_2)_\perp^4} (p_1^-)^2 \frac{1}{p_1^2 p_2^2} e^{-ip_2(x-y)} \\
&= \delta^{ab} i \frac{2N_c g^2 \lambda}{(2\pi)^7} (p_2^-)^2 \int d^4 p_2 \frac{1}{p_2^2} \int \frac{dp_1^+}{2p_1^+ p_2^- - p_{1\perp}^2 + i\epsilon} \int \frac{d^2 p_{1\perp}}{(p_1 - p_2)_\perp^4} e^{-ip_2(x-y)} \\
&= \delta^{ab} i \frac{2N_c g^2 \lambda}{(2\pi)^7} (p_2^-)^2 \int d^4 p_2 \frac{1}{p_2^2} \int \frac{dp_1^+}{2p_1^+ p_2^- - p_{1\perp}^2 + i\epsilon} \int \frac{d^2 k_\perp}{k_\perp^4} e^{-ip_2(x-y)}.
\end{aligned}$$

Identifying the integrals of p_1 and k_\perp as the same as of eq. (5.24) and (5.25),

and by changing p_2 to q , we finally have

$$\begin{aligned}
& \langle \partial_x^\mu g f^{bcd} A^{c\nu}(y) G_{\mu\nu}^{Iad}(x, y) \rangle \\
&= \delta^{ab} \frac{N_c g^2 \lambda}{8\pi} (\theta(q^-) - \theta(-q^-)) \frac{Q^2 - \Lambda_{QCD}^2}{\Lambda_{QCD}^2 Q^2} \int \frac{d^4 q}{(2\pi)^4} \frac{q^-}{q^2} e^{-iq(x-y)}. \quad (\text{B.32})
\end{aligned}$$

The second term of the $O(A^2)$ term has the same contribution as the first

term, as

$$\langle \partial_y^\nu g f^{ace} A^{c\mu}(x) G_{\mu\nu}^{Ieb}(x, y) \rangle \quad (\text{B.33})$$

$$= \delta^{ab} \frac{N_c g^2 \lambda}{8\pi} (\theta(q^-) - \theta(-q^-)) \frac{Q^2 - \Lambda_{QCD}^2}{\Lambda_{QCD}^2 Q^2} \int \frac{d^4 q}{(2\pi)^4} \frac{q^-}{q^2} e^{-iq(x-y)}. \quad (\text{B.34})$$

So the sum of the two is

$$\delta^{ab} \frac{N_c g^2 \lambda}{4\pi} (\theta(q^-) - \theta(-q^-)) \frac{Q^2 - \Lambda_{QCD}^2}{\Lambda_{QCD}^2 Q^2} \int \frac{d^4 q}{(2\pi)^4} \frac{q^-}{q^2} e^{-iq(x-y)}. \quad (\text{B.35})$$

For the last term in eq. (B.32), let us recall G_{11} of eq. (5.27) in coordinate space as

$$G_{11\mu\nu}^{+ab}(x, y) = g_{\mu\nu} \delta^{ab} \left(-\frac{g^2 N_c \lambda}{4\pi} \right) \frac{Q^2 - \Lambda_{QCD}^2}{\Lambda_{QCD}^2 Q^2} (\theta(q^-) - \theta(-q^-)) \frac{d^4 q}{(2\pi)^4} \frac{q^-}{q^4} e^{-iq(x-y)}. \quad (\text{B.36})$$

Applying the derivatives $\partial_x^\mu \partial_y^\nu$ provides $-iq^\mu i q^\nu$ which contracts with $g_{\mu\nu}$ gives q^2 canceling one of the q^2 in the denominator. Therefore, we have

$$\begin{aligned} & \partial_x^\mu \partial_y^\nu \langle G_{11\mu\nu}^{+ab}(x, y) \rangle_{MV} \\ &= \delta^{ab} \left(-\frac{g^2 N_c \lambda}{4\pi} \right) \frac{Q^2 - \Lambda_{QCD}^2}{\Lambda_{QCD}^2 Q^2} (\theta(q^-) - \theta(-q^-)) \frac{d^4 q}{(2\pi)^4} \frac{q^-}{q^2} e^{-iq(x-y)}, \end{aligned} \quad (\text{B.37})$$

which exactly cancel the sum of the first two $O(A^2)$ terms in (B.35). So we claim to the leading order in A , $O(A^2)$ and g , $O(g^2)$, the generalized Slavnov-Taylor identity for two point GF is satisfied by the modified gluon propagator obtained in Section 5.

Bibliography

- [1] K. Nakamura et al. *J. Phys. G*, 37:075021, 2010. and references therein.
- [2] D. Cline, F. Halzen, and J. Luthe. *Phys. Rev. Lett.*, 31:491, 1973.
- [3] J. R. Forshaw and D. A. Ross. *Quantum Chromodynamics and the Pomeron*. Cambridge University Press, 1997.
- [4] Keiji Igi and Satoshi Matsuda. New sum rules and singularities in the complex j plane. *Phys. Rev. Lett.*, 18(15):625–627, Apr 1967.
- [5] S. Chekanov et al. An NLO QCD analysis of inclusive cross-section and jet- production data from the zeus experiment. *Eur. Phys. J.*, C42:1–16, 2005.
- [6] David J. Gross and Frank Wilczek. Ultraviolet behavior of non-abelian gauge theories. *Phys. Rev. Lett.*, 30(26):1343–1346, Jun 1973.
- [7] H. David Politzer. Reliable perturbative results for strong interactions? *Phys. Rev. Lett.*, 30(26):1346–1349, Jun 1973.
- [8] John C. Collins, Davison E. Soper, and George F. Sterman. Factorization of Hard Processes in QCD. *Adv. Ser. Direct. High Energy Phys.*, 5:1–91, 1988.

- [9] K. Golec-Biernat and M. Wüsthoff. *Phys. Rev. D*, 59(1):014017, Nov 1998.
- [10] C. Chiu. *Ann. Rev. of Nucl. Science*, 22:255, 1972.
- [11] I. Ia Pomeranchuk. *Zh. Eksp. Teor. Fiz.*, 34:725, 1958. [Sov. Phys. JETP 7, 499 (1958)].
- [12] M. Froissart. *Phys. Rev.*, 123(3):1053, August 1961.
- [13] A. Martin. *Phys. Rev.*, 129(3):1432, February 1963.
- [14] A Sommerfeld. *Partial Differential Equation in Physics*. Academic Press, 1949.
- [15] S Mandelstam. *Annals of Physics*, 19:254, 1962.
- [16] H. Harari. *Phys. Rev. Lett.*, 20:1395, 1968.
- [17] R. Dolen, D. Horn, and C. Schmid. Finite-energy sum rules and their application to πn charge exchange. *Phys. Rev.*, 166(5):1768–1781, Feb 1968.
- [18] G. Veneziano. *Nuovo Cimento*, 57A:190, 1968.
- [19] Haim Harari. Duality diagrams. *Phys. Rev. Lett.*, 22(11):562–565, Mar 1969.
- [20] Jonathan L. Rosner. Graphical form of duality. *Phys. Rev. Lett.*, 22(13):689–692, Mar 1969.

- [21] G. Pancheri and C. Rubbia. *Nucl. Phys. A*, 418:117, 1984.
- [22] T. Gaisser and F. Halzen. *Phys. Rev. Lett.*, 54:1754, 1985.
- [23] L. Durand and H. Pi. *Phys. Rev. Lett.*, 58:303, 1987.
- [24] A. Capella, J. Kwiecinsky, and J. Tran Thahn. *Phys. Rev. Lett.*, 58:2015, 1987.
- [25] R.M. Godbole, A. Grau, G. Pancheri, and Y.N. Srivastava. *Phys. Rev. D*, 72:076001, 2005.
- [26] E.G.S. Luna, A.F. Martini, M.J. Menon, A. Mihara, and A.A. Natale. *Phys. Rev. D*, 72:034019, 2005.
- [27] Andrea Achilli et al. *arXiv:1102.1949*, 2011.
- [28] Yu. L. Dokshitzer. *Sov. Phys. JETP*, 73:1216, 1977.
- [29] V. N. Gribov and L. N. Lipatov. *Sov. J. Nucl. Phys.*, 15:78, 1972.
- [30] G. Altarelli and G. Parisi. *Nucl. Phys. B*, 126:298, 1977.
- [31] C. Adloff et al. *Eur. Phys. J.*, C21:33–61, 2001.
- [32] S. Chekanov et al. *Nucl. Phys.*, B831:1–25, 2010.
- [33] S. Donnachie, G. Dosch, P. Landshoff, and O. Nachtmann. *Pomeron Physics and QCD*. Cambridge Univ. Press, 2002.

- [34] E. Iancu, A. Leonidov, and L. McLerran. The Colour Glass Condensate: An Introduction. *arXiv:hep-ph/0202270*, February 2002.
- [35] L. McLerran and R. Venugopalan. *Phys. Rev. D*, 49(5):2233, March 1994.
- [36] L. McLerran and R. Venugopalan. *Phys. Rev. D*, 49(7):3352, April 1994.
- [37] L. McLerran and R. Venugopalan. *Phys. Rev. D*, 50(3):2225, August 1994.
- [38] I. Baltisky and L.N. Lipatov. *Sov. J. Nucl. Phys.*, 28:822, 1978.
- [39] E.A. Kuraev, L.N. Lipatov, and V.S. Fadin. *Sov. Phys. JETP*, 45:199, 1977.
- [40] Edmond Iancu, Andrei Leonidov, and Larry McLerran. *Nucl. Phys.*, A692:583, 2001.
- [41] L. F. Abbott. *Nucl. Phys.*, B185:189, 1981. and references therein.
- [42] Ina Sarcevic, Stephen D. Ellis, and Peter Carruthers. Qcd minijet cross sections. *Phys. Rev. D*, 40(5):1446–1452, Sep 1989.
- [43] Stefan Kluth. *Reports on Progress in Physics*, 69(6):1771, 2006.
- [44] J. Bartels, K. Golec-Biernat, and H. Kowalski. *Phys. Rev. D*, 66(1):014001, Jun 2002.

- [45] Edmond Iancu, K Itakura, and S Munier. *Phys. Lett. B*, 590:199–208, 2004.
- [46] Edmond Iancu and Raju Venugopalan. *arXiv: hep-ph/0303204*, 2003.
- [47] Francois Gelis, Edmond Iancu, Jamal Jalilian-Marian, and Raju Venugopalan. The Color Glass Condensate. *Ann. Rev. Nucl. Part. Sci.*, 60:463–489, 2010.
- [48] J. P. Blaizot. The Status of Parton Saturation and the CGC. *Nucl. Phys.*, A854:237–256, 2011.
- [49] Alex Kovner, Larry D. McLerran, and Heribert Weigert. Gluon production from nonAbelian Weizsacker-Williams fields in nucleus-nucleus collisions. *Phys. Rev.*, D52:6231–6237, 1995.
- [50] M. Gyulassy and Larry D. McLerran. Yang-Mills radiation in ultrarelativistic nuclear collisions. *Phys. Rev.*, C56:2219–2228, 1997.
- [51] Adrian Dumitru and Larry D. McLerran. How protons shatter colored glass. *Nucl. Phys.*, A700:492–508, 2002.
- [52] Dmitri Kharzeev and Marzia Nardi. Hadron production in nuclear collisions at RHIC and high density QCD. *Phys.Lett.*, B507:121–128, 2001.
- [53] Dmitri Kharzeev and Eugene Levin. Manifestations of high density QCD in the first RHIC data. *Phys. Lett.*, B523:79–87, 2001.

- [54] Dmitri Kharzeev, Yuri V. Kovchegov, and Kirill Tuchin. Nuclear modification factor in $d + \text{Au}$ collisions: Onset of suppression in the color glass condensate. *Phys. Lett.*, B599:23–31, 2004.
- [55] Dmitri Kharzeev, Eugene Levin, and Marzia Nardi. Qcd saturation and deuteron-nucleus collisions. *Nuclear Physics A*, 730(3-4):448 – 459, 2004.
- [56] D. Kharzeev, E. Levin, and M. Nardi. *Nucl. Phys. A*, 747:609–629, 2005.
- [57] François Gelis and Jamal Jalilian-Marian. *Phys. Rev. D*, 66(1):014021, Jul 2002.
- [58] François Gelis and Jamal Jalilian-Marian. *Phys. Rev. D*, 66(9):094014, Nov 2002.
- [59] F. Gelis and A. Peshier. *Nucl. Phys. A*, 697(3-4):879 – 901, 2002.
- [60] F. Gelis and A. Peshier. *Nucl. Phys. A*, 707(1-2):175 – 192, 2002.
- [61] Jean-Paul Blaizot, Francois Gelis, and Raju Venugopalan. *Nucl. Phys. A*, 743(1-3):13, 2004.
- [62] Jean Paul Blaizot, Francois Gelis, and Raju Venugopalan. *Nucl. Phys.*, A743:57, 2004.
- [63] A. A. Slavnov. *Theor. Math. Phys.*, 10:99, 1972. Our work involves a classical field. For a version without classical field, see this reference.
- [64] J. C. Taylor. *Nucl. Phys.*, B33:436–444, 1971.

- [65] Q. Wang, K. Redlich, H. Stöcker, and W. Greiner. Kinetic equation for gluons in the background gauge of qcd. *Phys. Rev. Lett.*, 88(13):132303, Mar 2002.